Department of Construction Sciences
Solid Mechanics

ISRN LUTFD2/TFHF-22/5246-SE(1-81)

Parameter study of the diagonal on a gasketed plate heat exchanger

Master's Dissertation by

Benjamin Kabil

Supervisors:
Håkan Hallberg, Division of Solid Mechanics
Joakim Krantz, Alfa Laval

Examiner:
Mathias Wallin, Division of Solid Mechanics

Abstract

The aim of this thesis is to further develop the understanding of how different parameters related to the gasket groove of a heat exchanger affect the mechanical performance of the product. Three different parameters with two different gasket materials were evaluated. Comparisons between the parameters where mainly made in terms of contact- and leakage pressure but phenomena related to factors such as stress and strain were also studied for explanatory reasons. The parameters were mainly analyzed in two steps that included forming of the plates and a final gasket simulation. In the gasket simulation, the plates were first compressed onto each other with the gasket in between them. After the compression, an internal fluid pressure was added to the geometry.

From the results it was found that the parameters cannot solely be analyzed from a plate perspective but that the relationship between the gasket and the plate geometry has a major role in the outcome of the results. The incompressibility of the rubber material used in the gasket is a factor that has to be accounted for when designing a gasket groove.

Contents

A Result plots

1 Introduction

1.1 Alfa Laval

Alfa Laval is a global provider of products in the areas of heat transfer, separation and fluid handling. The company was founded in 1883 by Gustav de Laval shortly after the introduction of the first centrifugal separator. The company was founded with the name AB Separator. In 1938, Alfa Laval introduced it's first heat exchanger. The development and production was established in Lund, where it is currently located. The company changed its name from AB Separator to Alfa-Laval AB 1963. "Alfa" stems from the Alfa discs that are used in the separators. Laval is in honor of the founder, Gustav de Laval [5].

1.2 Background

There are many different types of heat exchangers, in this thesis mainly gasketed plate heat exchangers (GPHE) are examined. The GPHE consists of a frame plate, a pressure plate and a number of channels in between the frame- and pressure-plates that are separated with rubber gaskets. The gaskets do not only separate the plates from each other, but also play a major role in directing the flow between the plates. The plates are designed with grooves where the gasket is later on placed.

The performance of a GPHE is mainly measured in terms of mechanical performance and thermal performance. When measuring the mechanical performance of the heat exchanger, the contact pressure and leakage pressure are the most interesting parameters. The contact pressure is defined as the pressure between the plates and the gaskets. The leakage pressure is determined as the internal pressure required for fluid to leak from the GPHE.

1.3 Aim

During the design process of the channel plates for a heat exchanger, the gasket grooves are of significant interest. Currently, there exists no data on how different parameters associated with the gaskets and gaskets grooves affect the mechanical and thermal performance of the heat exchanger. A better understanding of these parameters could aid the engineers in their design process associated with the channel plates.

The task at hand is to examine different parameters of the gasket and gasket groove with respect to primarily mechanical performance. The goal is to develop a model that the designers can use when designing channel plates for Alfa Laval's © heat exchangers.

1.4 Confidential information

Some of the material in this report has been removed due to confidentiality. This includes sensitive data such as numerical values related to the material models of the gaskets, dimensions of parameters related to the geometry of the gasket and values of the results in terms of leakage pressure and contact pressure. In other terms, this means that some information will not be as detailed as it perhaps could have been. The results will be presented in general terms and some specific details regarding the products will not be disclosed.

2 Theory

In this chapter, necessary theory needed to understand the project is introduced. At first, theory related to the heat exchanger and the geometry of the gasket groove will be introduced.

2.1 The Heat exchanger

This master thesis is focused around the gasket plate heat exchanger. The main purpose of a heat exchanger is to transfer heat from one fluid to another. The gasket plate heat exchanger consists of a number of metal plates stacked onto each other. The plates are separated by a small gap created by the gaskets. This gap serves as channels where the fluids can pass. The fluids are directed with gaskets in order to alternate between the plates. This is illustrated in figure 1 where the red fluid represents the hot fluid and the blue represents the cold fluid.

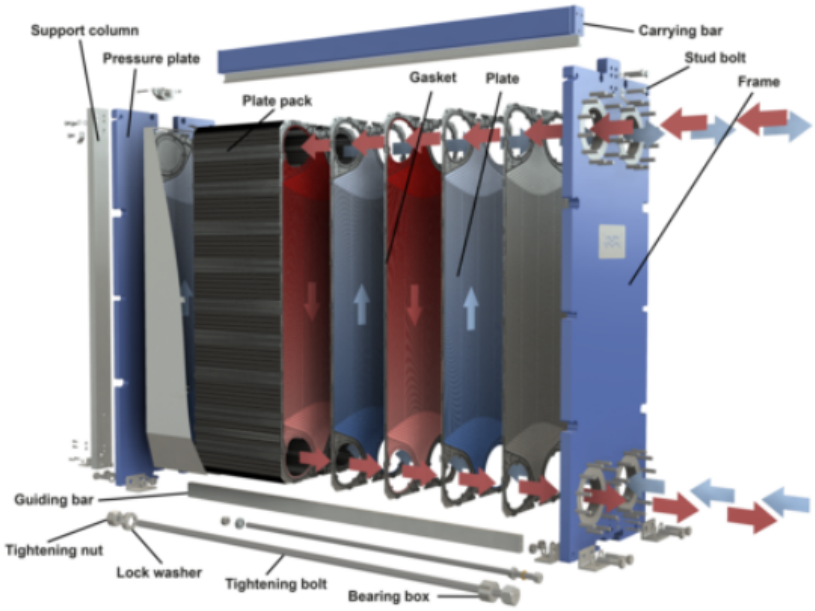

Figure 1: *Working principles of a gasket heat exchanger [4]*

2.2 General plate theory

The channel plates are the most critical parts for the functioning of the GPHE. It is through them that the heat transfer between the fluids occur. The channel plates are built with a complex pattern that is made in order for the fluid to flow as desired and to optimize the heat transfer for the heat exchanger. The pattern is divided into different sections that are illustrated in figure 2.

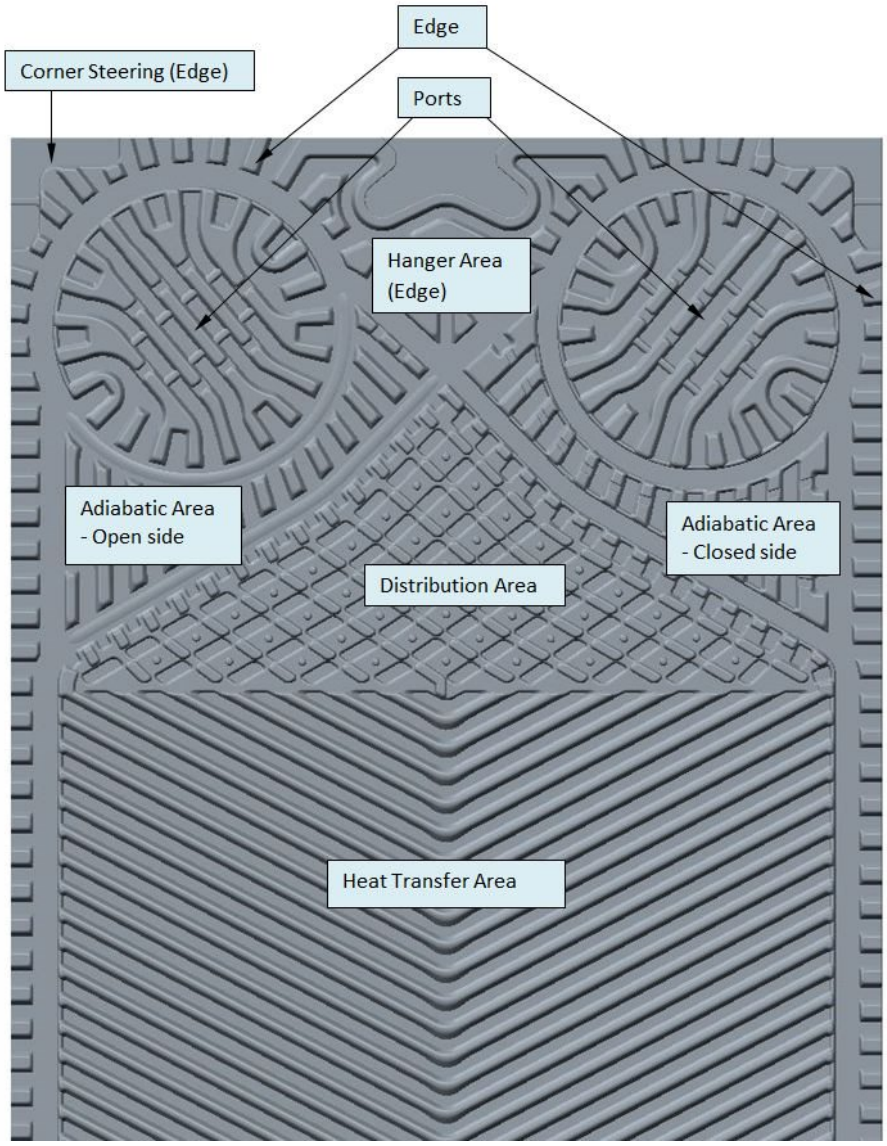

Figure 2: *Different sections illustrated on a channel plate*

The ports on the plate can either be open or closed, as shown in figure 2. The ports enable the fluid to flow across the heat exchanger. The adiabatic area together with the distribution area is where the fluid is directed to the heat transfer area. On the closed side of the plate, gaskets are placed in the groove between the adiabatic- and distribution area to block the fluid from reaching the heat transfer area. This groove is called the diagonal groove, marked in figure 3. The diagonal groove on the open side does not have a gasket and thus the fluid coming from the port connected to that side can travel freely to the heat transfer area.

2.2.1 Gasket grooves

The gaskets are placed in grooves located on the metal plates. The grooves provide support for the gasket so that it is unable to move across the plate. The gasket is divided into different regions. In general these grooves include the diagonal gaskets and the field gaskets. The field gaskets appear between every plate in the heat exchanger and are mainly used to keep the fluids inside the heat exchanger. The diagonal gaskets are used to direct the flow of the fluids and are placed between the adiabatic- and distribution area on the closed side, see figure 2. The gaskets along with their grooves are divided into three main sections, namely the field gaskets, the diagonal gaskets and the ring gaskets. Figure 3 illustrates where the different sections are located on the plate.

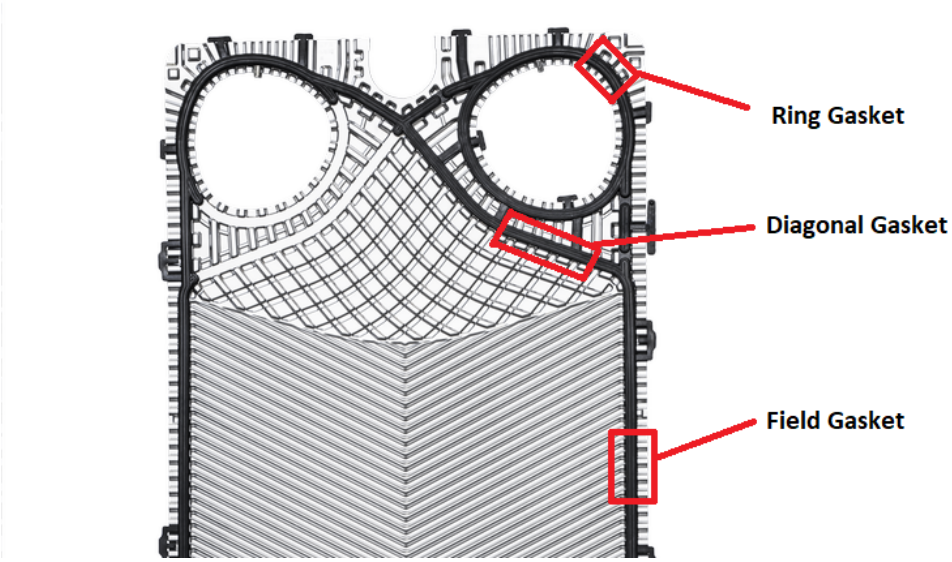

Figure 3: *Gasket type locations, shown on a channel plate*

2.2.2 Diagonal groove

The diagonal section is of particular interest when performing analyses related to the mechanical performance of the heat exchanger. Since the diagonal gasket only appears on alternating sides of the plate, the region around the diagonal section experiences particularly high stresses when the plates are compressed onto each other. The diagonal is used to block the fluid from the distribution surface from entering the channel of the other fluid.

2.3 Design parameters - Gasket and gasket groove

There are many different parameters to consider when designing a gasket groove with a gasket. Change of these parameters can have large effects on the mechanical performance of the GPHE. In this section, the most commonly referred to parameters will be introduced and their significance will be described.

2.3.1 Line elongation

The line elongation is defined as the difference in length between two fixed points of the plate before and after pressing. Figure 4 illustrates how these lengths are defined. The elongation is derived by dividing the distance B with the distance A. Large values on the line elongation can result in the material cracking during the pressing of the plates.

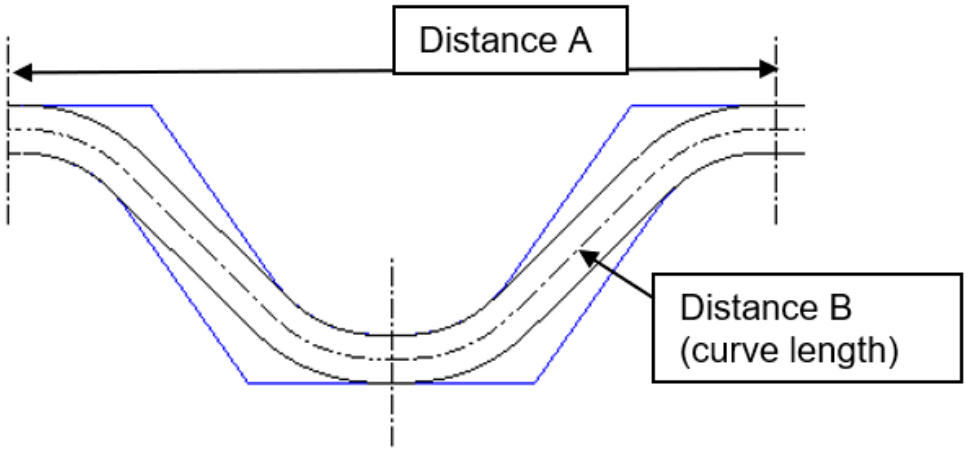

Figure 4: *Example of line elongation*

2.3.2 Filling ratio

The filling ratio is given by the gasket section area divided by the gasket groove section area. The gasket groove section area is defined with the free channel height. The filling ratio has a major impact on quantities such as contact pressure and equivalent stresses. Figure 5 illustrates the different parameters that are used to calculate the filling ratio.

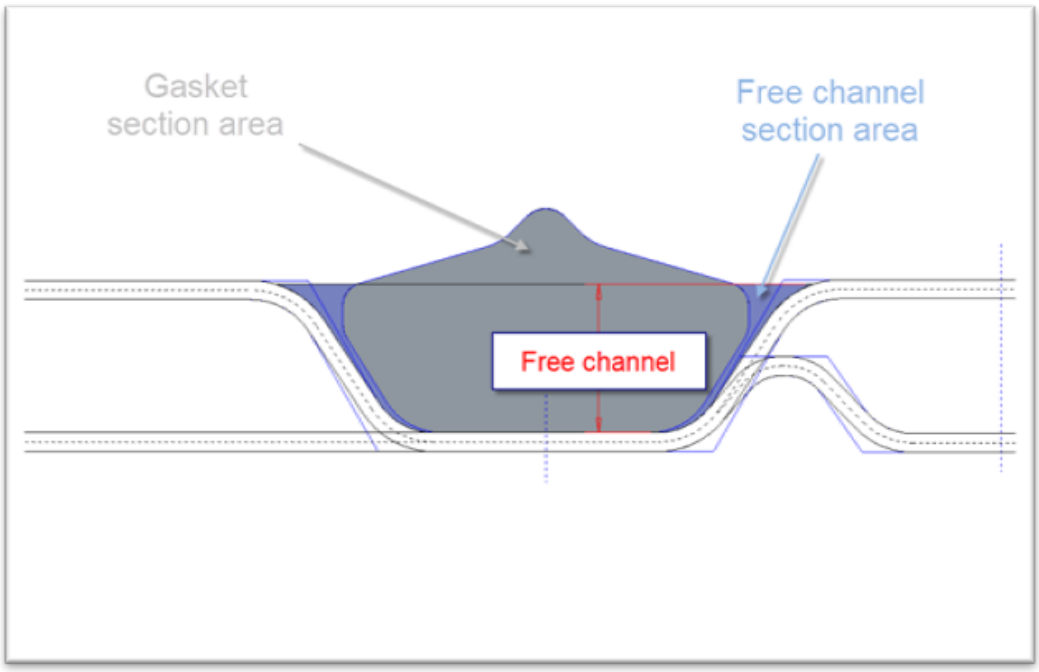

Figure 5: *Gasket cross section area and free channel cross section area*

2.3.3 Line load

Line load is defined according to equation (1). The load that the gasket exhibits on the plate is divided by the total length of the gasket.

$$Line\ load = \frac{Gasket\ load}{Gasket\ length} \tag{1}$$

2.4 Mechanical performance of GPHE

There are many different parameters that can be used to determine the mechanical performance of the heat exchanger, depending on what is of interest. This thesis is constrained to evaluating the contact pressure and the leakage pressure. The contact pressure describes the pressure that is exerted on the gasket by the plates during compression of the plate package and as the internal pressure is applied. The leakage pressure describes the maximum internal pressure that can be applied to the heat exchanger without the leakage occurring in the gasket. Parameters such as equivalent stress can be interesting when analyzing plastic behaviour in the plates or crushing of the gasket.

2.5 The Finite Element method

The finite element method will be the main tool when simulating the gasket and the gasket groove. All the physical phenomena that we encounter in this problem require differential

equations to be modelled and solved. The problems are too complicated to be solved by analytical methods. The finite element method can be used to approximately solve a large number of differential equations for complex geometries. Instead of finding a general solution for the entire geometry, the geometry is divided into so called finite elements, and the differential equations are solved locally for each element [6].

2.5.1 Strong formulation

The equations of motion are of fundamental importance for solid mechanics and therefore will be used in deriving the FE-formulation for this problem. To formulate the strong form of the problem, an arbitrary body with volume V and outer surface S is fist introduced. The outer forces acting on the surface S are summarized in the traction vector t_i and body forces acting on per unit volume in the volume V are summarized in the vector b_i. The displacement vector is denoted by u_i and the acceleration vector then becomes $\ddot{u}_i$. From Newton's second law the following relation is obtained

$$\int_S t_i dS + \int_V b_i dV = \int_V \rho \ddot{u}_i dV \tag{2}$$

The Gauss divergence theorem states that the following should hold for an arbitrary quantity $\boldsymbol{q}$

$$\int_V q_{i,i} dV = \int_S q_i n_i dS \tag{3}$$

Where $\boldsymbol{n}$ denotes the surface normal.For an arbitrary quantity c_{ij}, equation (3) can be rewritten as

$$\int_V c_{ij,j} dV = \int_S c_{ij} n_j dS \tag{4}$$

With this expression, equation (2) can be reformulated to

$$\int_V (\sigma_{ij,j} + b_i - \rho \ddot{u}_i) dV = 0 \tag{5}$$

Since equation (5) holds for arbitrary regions V, the following can be concluded

$$\sigma_{ij,j} + b_i = \rho \ddot{u}_i \tag{6}$$

Which is the equation of motion, and also the strong formulation of the problem [7].

2.5.2 Weak formulation

The next step in obtaining the FE-approximation of the problem is to derive the weak form. The first step in doing this is to multiply equation (6) with an arbitrary weight vector v_i and then integrate over the volume V according to

$$\int_V v_i(\sigma_{ij,j} + b_i - \rho\ddot{u}_i)dV = 0 \tag{7}$$

This can be rewritten to the following relation

$$\int_V \left[(\sigma_{ij}v_i)_{,j}) - \sigma_{ij}v_{i,j}\right] dV + \int_V (v_i b_i - \rho v_i \ddot{u}_i)dV = 0 \tag{8}$$

Recalling the divergence theorem of Gauss, the following relation is obtained

$$\int_V (\sigma_{ij}v_i)_{,j})dV = \int_S \sigma_{ij}v_i n_j dS = \int_S v_i t_i dS \tag{9}$$

Combining this relation with equation (7) results in the following relation

$$\int_V \rho v_i \ddot{u}_i dV + \int_V v_{i,j}\sigma_{ij}dV = \int_S v_i t_i dS + \int_V v_i b_i dV \tag{10}$$

An arbitrary tensor can be defined in the following way

$$\varepsilon^v_{ij} = \frac{1}{2}(v_{i,j} + v_{j,i}) \tag{11}$$

The relation for this tensor is the same as for the relationship between the strain tensor ε_{ij} and the displacement vector u_i. The difference is that the "strain" now is associated with the arbitrary vector v_i.

The tensor σ_{ij} is symmetrical and due to this symmetry the following can be established

$$v_{i,j}\sigma_{ij} = \frac{1}{2}(v_{i,j}\sigma_{ij} + v_{j,i}\sigma_{ji}) = \frac{1}{2}(v_{i,j}\sigma_{ij} + v_{j,i}\sigma_{ij}) = \varepsilon^v_{ij}\sigma_{ij} \tag{12}$$

This relation can now be used to rewrite equation (10) into

$$\int_V \rho v_i \ddot{u}_i dV + \int_V \varepsilon^v_{ij}\sigma_{ij}dV = \int_S v_i t_i dS + \int_V v_i b_i dV \tag{13}$$

This is the weak form of the problem and it is fundamental when deriving the FE-approximation for the equations of motion [7].

2.5.3 FE-approximation

Returning to a matrix format, the weak form in equation (13) can be rewritten as

$$\int_V \rho \boldsymbol{v}^T \ddot{\boldsymbol{u}} dV + \int_V (\boldsymbol{\varepsilon}^v)^T \boldsymbol{\sigma} dV = \int_S \boldsymbol{v}^T \boldsymbol{t} dS + \int_V \boldsymbol{v}^T \boldsymbol{b} dV \tag{14}$$

The displacement vector $\boldsymbol{u}$ can be approximated with the following relation

$$\boldsymbol{u} = \boldsymbol{N}\boldsymbol{a} \tag{15}$$

Where $\boldsymbol{N}$ is the global shape function and $\boldsymbol{a}$ is the column matrix that includes the nodal displacements of the body.

The displacement vector $\boldsymbol{u}$ is both position and time dependent while the global shape functions is only position dependent. Therefore equation (15) can be rewritten as

$$\ddot{\boldsymbol{u}} = \boldsymbol{N}\ddot{\boldsymbol{a}} \tag{16}$$

The strain vector follows in the same way, and the following relation is obtained

$$\varepsilon = \boldsymbol{B}\boldsymbol{a} \tag{17}$$

Where the matrix $\boldsymbol{B}$ is derived from the global shape functions.

The arbitrary weight vector $\boldsymbol{v}$ is chosen following the Galerkin method, meaning that it is approximated in the same way as with the displacement $\boldsymbol{u}$. The weight function can be approximated as

$$\boldsymbol{v} = \boldsymbol{N}\boldsymbol{c} \tag{18}$$

The vector $\boldsymbol{c}$ is arbitrary since $\boldsymbol{v}$ is arbitrary. Using this relation, the vector $\boldsymbol{\varepsilon^v}$ can be determined in a similar way as for equation (17) according to

$$\boldsymbol{\varepsilon^v} = \boldsymbol{B}\boldsymbol{c} \tag{19}$$

Using equation (18) and equation (19) into equation (14) yields the following relation

$$\boldsymbol{c^T}\left[\int_V (\rho \boldsymbol{N^T}\boldsymbol{N} dV)\ddot{\boldsymbol{a}} + \int_V \boldsymbol{B^T}\boldsymbol{\sigma} dV - \int_S \boldsymbol{N^T}\boldsymbol{t} dS - \int_V \boldsymbol{N^T}\boldsymbol{b} dV\right] = 0 \tag{20}$$

Since $\boldsymbol{c}$ is arbitrary the following should hold

$$\boldsymbol{M}\ddot{\boldsymbol{a}} + \int_V \boldsymbol{B^T}\boldsymbol{\sigma} dV = \boldsymbol{f} \tag{21}$$

Where $\boldsymbol{M}$ is the mass matrix and is defined according to

$$\boldsymbol{M} = \int_V \rho \boldsymbol{N^T}\boldsymbol{N} dV \tag{22}$$

The vector $\boldsymbol{f}$ contains the external force and is defined as

$$\boldsymbol{f} = \int_S \boldsymbol{N^T t} dS \int_V \boldsymbol{N^T b} dV \tag{23}$$

Equation (21) forms the basis of for the algorithms that are used in the analyses for this thesis [7].

2.6 Non-linear approach

In this type of problem, there are many different non-linearities that occur. For instance, the gasket itself is made of a special kind of rubber that behaves in a non-linear manner when compressed. The plates located on each side of the rubber will be plastically deformed which in itself is a non-linear behaviour. These non-linearities result in the need to use non-linear methods during the finite element analysis of this problem. In this subsection, the algorithm that will be used will be explained in detail.

2.6.1 Newton-Raphson method

The Newton-Raphson method is an iterative algorithm. The goal of the Newton-Raphson method is to eliminate the errors that accumulate on each step when using for instance the Euler explicit method. The most general form of the Newton-Raphson method is based on two steps. The first step is to check if equilibrium is obtained for a given tolerance. If the first step is not satisfied, the algorithm is to perform the second step, i.e. to make adjustments to the state of deformation until equilibrium is obtained.

The equilibrium conditions is satisfied if the following condition holds

$$r(u, f) = f - g(u) = 0 \tag{24}$$

In equation (24), $r(u, f)$ denotes the residual and is a function of the external force f and the displacement u. The function $g(u)$ is the internal force and is also a function of the displacement. The condition states that the difference between the internal and external forces should be zero. For instance, in the beginning of a load increment, equation (24) will not be fulfilled since there is no estimate of the displacement available. In this case, the algorithm needs to proceed to the second step of the iteration. The unknown displacement u is obtained from a linearized residual $r(u+\delta u, f)$ around the residual $r(u, f)$. The linearized residual is defined as

$$r(u + \delta u, f) = r(u, f) + \delta r(u, f) + (H.O.)... = 0 \tag{25}$$

Where H.O. stands for higher order terms. In this case the load f is fixed around a given load step and the increment of the residual only depends on the internal forces according to

$$\delta r = \frac{dg(u)}{du}\delta u = -K(u)\delta u \tag{26}$$

Where K is the tangent stiffness and describes the change of force for a given change of displacement. By applying equation (26) into equation (25) and rearranging the terms the following relation is obtained

$$K(u)\delta u = r \Longleftrightarrow \delta u = K^{-1}(u)r \tag{27}$$

This relation can as seen be used to determine the displacement increment which is then used to update the current displacement according to

$$u^i = u^{i-1} + \delta u^i \tag{28}$$

The entire process is illustrated in figure 6. Here it can be seen that the load step starts from a state of equilibrium that has already been established and then increases with a increment Δf_n to the next step. From this step, the first residual is obtained and it in turn can be used to establish the first displacement increment δu_n^1. At the second displacement obtained from $u_n^{-1} + \delta u_n^1$ the internal force vector g is still smaller than the imposed load and a new residual is formed. The process is repeated until a given tolerance on the residual in equation (24) is fulfilled [3].

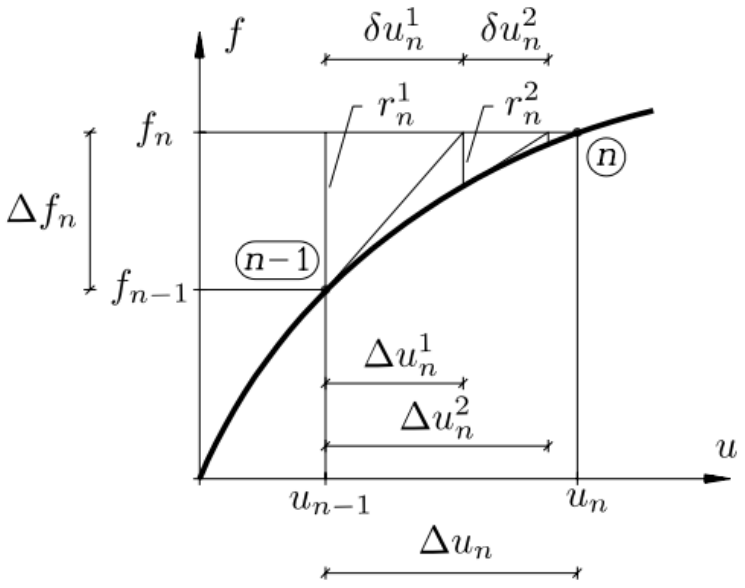

Figure 6: *Illustration of the Newton-Raphson algorithm*

Figure 7 illustrates the Newton-Raphson procedure in a step by step scheme. The tolerance

is normally chosen to a value between 10^{-4} and 10^{-6}.

-

Load steps $n = 1, 2, \ldots, n_{\max}$

$\mathbf{f}_n = \mathbf{f}_{n-1} + \Delta\mathbf{f}_n$

$\mathbf{u}_n = \mathbf{u}_{n-1}$

Iterations $i = 1, 2, \ldots, i_{\max}$

$\mathbf{K}_n = \dfrac{d\mathbf{g}(\mathbf{u}_n)}{d\mathbf{u}}$

$\mathbf{r}_n = \mathbf{f}_n - \mathbf{g}(\mathbf{u}_n)$

$\delta\mathbf{u}_n = \mathbf{K}_n^{-1}\mathbf{r}_n$

$\mathbf{u}_n = \mathbf{u}_n + \delta\mathbf{u}_n$

Stop iteration when $\|\mathbf{r}_n\| < \epsilon \|\Delta\mathbf{f}_n\|$

End of load step

Figure 7: *Procedure when performing the Newton-Raphson algorithm*

2.7 Contact modelling

The problem in this dissertation is highly focused on contact modelling. The gasket present in the analysis is essentially clamped between two plates before the pressure is applied. To be able to capture the behaviour correctly, the simulation model needs to be modified to include contact.

There are different ways of modelling the contact between bodies. In this thesis, a penalty based method will be used. The method is based on adding a penalty term to the solution algorithm. To derive this formulation, a contact between a deformable body and a rigid wall is first considered. The potential energy for this problem is given by

$$\Pi = \int_{V_0} \varphi dV_0 - \int_{S_0} \boldsymbol{u}^{\boldsymbol{T}} \boldsymbol{t}^{\boldsymbol{0}} dS_0 - \int_{V_0} \boldsymbol{u}^{\boldsymbol{T}} \boldsymbol{b}^{\boldsymbol{0}} dV_0 + \int_{S_0^C} \frac{\varepsilon_N}{2} \overline{g}_N^2 dS_0^c \tag{29}$$

Where the last term is related to penetration between the bodies, as seen in figure 8.

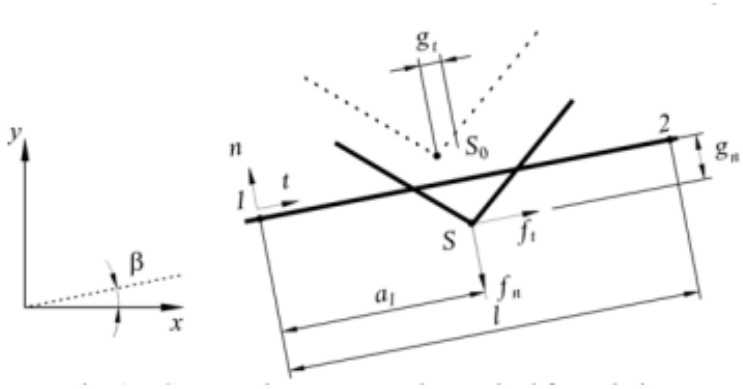

Figure 8: *Contact elements, penetration between bodies*

The term ε_N is a penalty parameter. From this expression, the virtual work is derived as

$$\int_{V_0} \delta \boldsymbol{E}^{\boldsymbol{T}} \boldsymbol{S} dV_0 = \int_{S_0} \delta \boldsymbol{u}^{\boldsymbol{T}} \boldsymbol{t}^{\boldsymbol{0}} dS_0 + \int_{V_0} \delta \boldsymbol{u}^{\boldsymbol{T}} \boldsymbol{b}^{\boldsymbol{0}} dV_0 + \int_{S_c^0} \delta \boldsymbol{u}^{\boldsymbol{T}} \boldsymbol{t}^{\boldsymbol{c}} dS_0^c \tag{30}$$

Where the contact traction and the contact pressure are defined as

$$\begin{aligned} \boldsymbol{t}^{\boldsymbol{c}} &= t_N \boldsymbol{n} \\ t_N &= \varepsilon_N \overline{g}_N \end{aligned} \tag{31}$$

The residual to be minimized is then given by the following relation

$$\boldsymbol{r} = f_{int} - f_{ext} - f_{contact} \tag{32}$$

The internal, external and contact force vectors are defined in the following way:

$$\begin{aligned} \boldsymbol{f_{int}} &= \int_{V_0} \boldsymbol{B_0^T S} dV_0 \\ \boldsymbol{f_{ext}} &= \int_{S_0} \boldsymbol{N^T t^0} dS_0 + \int_{V_0} \boldsymbol{N^T b^0} dV_0 \\ \boldsymbol{f_{contact}} &= \int_{S_0^c} \boldsymbol{N^T t^c} dS_0^c \end{aligned} \tag{33}$$

By linearizing the equation (30), the contribution to the stiffness matrix due to contact can be derived as

$$\boldsymbol{K_c} = \int_{S_c} \varepsilon_N \boldsymbol{N^T} [\boldsymbol{n n^T} + Q_{\alpha\beta} \cdot (\overline{\boldsymbol{a}}_{\boldsymbol{\alpha}}^{\boldsymbol{w}} \overline{\boldsymbol{a}}_{\boldsymbol{\beta}}^{\boldsymbol{wT}})] \boldsymbol{N} dS \tag{34}$$

Where $\boldsymbol{a^w}$ is defined as the tangent vector [8].

2.8 Friction modelling

In the contacts between bodies, frictional effects are important aspects that need to be modelled. The most common and well known frictional model is the Coulomb frictional model. The Coulomb friction force is of a constant magnitude and acts in the opposite direction of motion. Even though the model may be an oversimplification of the real frictional phenomenons, it is well suited for static applications. The frictional force F_c is given by

$$F_c = \mu F_N \tag{35}$$

Where μ is the coefficient of friction and F_N is the normal force acting on the body. The Coulomb friction is illustrated in figure 9.

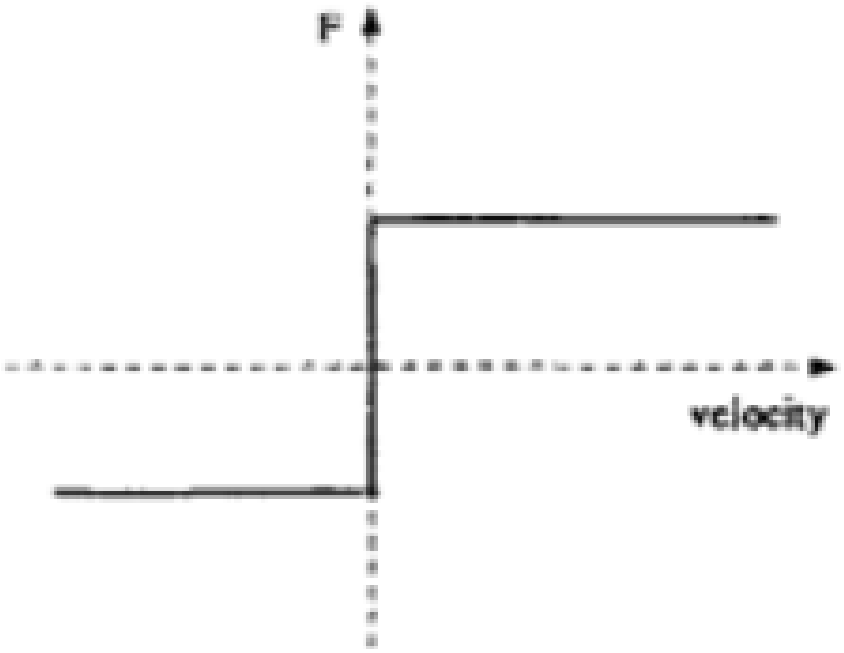

Figure 9: *Illustration of the Coulomb frictional model*

There are many different ways to model friction. One can for instance account for phenomenons such as viscous and static friction. More advanced models that are used in dynamic models account for the Stribeck effect, illustrated in figure 10.

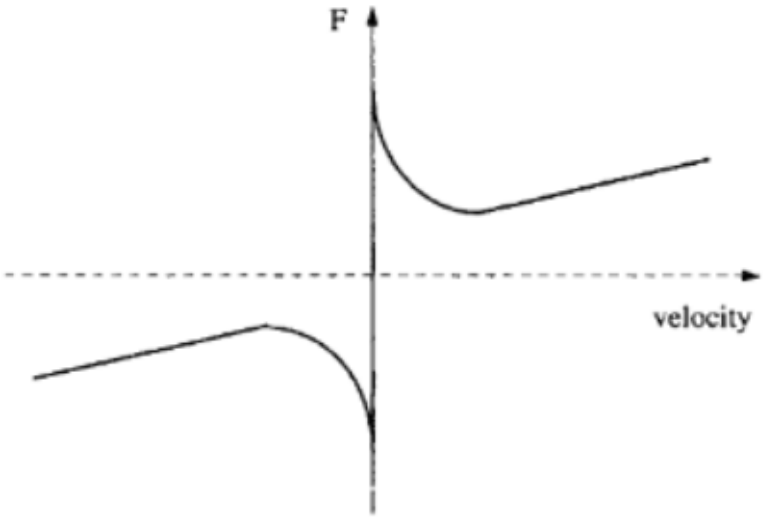

Figure 10: *Illustration of the Stribeck effect*

The Stribeck effect presents highly non-linear phenomenons around zero velocity, that can be very difficult to model [9].

2.9 Implicit and Explicit methods

For dynamic analyses, it is important to differentiate between explicit and implicit methods of solving differential equations. In general the implicit methods are better suited for problems with longer duration while the explicit methods are better approaches when solving problems with shorter duration and highly non-linear problems, such as those involving contacts.

2.9.1 Implicit methods

Implicit methods solve the differential equations by solving the equations for the current state and the next state. The advantages with this method is that it can effectively solve equations with a large time step. An example of an implicit method is the Euler backward method

$$Y_{k+1} = Y_k + f(t_k, Y_{k+1})\Delta t \tag{36}$$

Where it can be seen that both the current and next states are included in the solution (Y_k and Y_{k+1}). A disadvantage of this method is that it requires establishment of the full tangent stiffness and an iterative solution scheme [2].

2.9.2 Explicit methods

The working principle of the explicit methods is that they calculate the next state of the system exclusively from the current state. The forward Euler's method is an example of an explicit method. The next state is calculated with the following relation

$$Y_{k+1} = Y_k + f(t_k, Y_k)\Delta t \tag{37}$$

The disadvantage of the explicit methods lies in that the time step is only conditionally stable and usually very small time steps are required, leading to longer simulation times than when using implicit methods.

2.10 Material modelling

The relation between stresses and strains is provided by the constitutive relation.

2.10.1 Yeoh model

The gasket that is used in the heat exchangers is made of a special rubber compound. To accurately model the behaviour of the rubber, a hyperelastic material model originally developed O.H. Yeoh was used. The stress strain curve for the model can be seen in figure 11 . It can be noted that for biaxial loading, the stress increases dramatically upon reaching a certain value. In this thesis, two different rubber compounds are investigated for the gasket, namely the EPDM and NBRP rubber compounds. The model shown in the figure is associated with the NBRP rubber compound, but the general behaviour of the model is the same for the EPDM rubber compound that is also tested in this thesis. The main difference between the compounds is that the EPDM compound is stiffer than the NBRP.

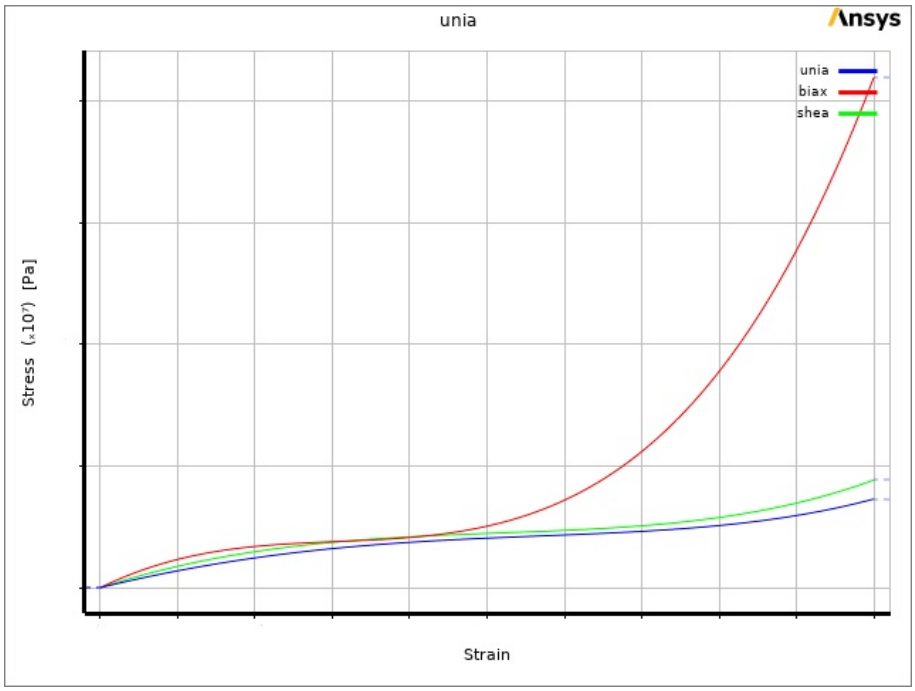

Figure 11: *Stress-strain plot for the 3d order Yeoh model shown for uniaxial (blue line), biaxial (red line) and shear (green line) loading, calibrated for the NBRP rubber compound*

The Yeoh model is especially adapted for incompressible rubber like materials. The strain energy for the model is given by the following relation

$$W = \sum_{i=1}^{N} \tilde{C}_i (I_1 - 3)^i \tag{38}$$

Where $\tilde{C}_i$ is a constant. Here it can be seen that the model assumes that the strain energy function is independent of the second strain invariant. For a first order series, the Yeoh model reduces to the Neo-Hookean model. The higher order terms in the Yeoh model allows the model to match better with experimental data. In this theis, a third order Yeoh model was used with constants specially adapted to the rubber compound used in Alfa Laval's gaskets [**3**].

2.11 Material type 36 - Barlat and Lian

The Material type 36 model was developed by Barlat and Lian to model sheets of anisotropic materials during plane stress conditions. Since the forming simulation discussed in section 4 describes this scenario, the model is deemed to be well suited for this application. The yield criterion is given by

$$f = a|K_1 + K_2|^m + a|K_1 - K_2|^m + c|2K_2|^m = 2\sigma_y^m \tag{39}$$

Where a and c are parameters related to the degree of anisotropy. And K_1 and K_2 are given from the following relation

$$\begin{aligned} K_1 &= \frac{\sigma_x + h\sigma_y}{2} \\ K_2 &= \sqrt{(\frac{\sigma_x - h\sigma_y}{2})^2 + p^2\tau_{xy}^2} \end{aligned} \tag{40}$$

The parameter p is obtained implicitly. The constants a, c and h are given by

$$\begin{aligned} a &= c - 2 = 2 - 2\sqrt{\frac{R_{00}}{1+R_{00}}\frac{R_{90}}{1+R_{90}}} \\ h &= \sqrt{\frac{R_{00}}{1+R_{00}}\frac{1+R_{90}}{R_{90}}} \end{aligned} \tag{41}$$

The R_ψ value that is the width to thickness strain ratio can for any angle ψ be obtained from

$$R_\psi = \frac{2m\sigma_Y^m}{(\frac{\partial\psi}{\partial\sigma_x} + \frac{\partial\psi}{\partial\sigma_y}\sigma_\psi)} - 1 \tag{42}$$

Where σ_ψ is the tension in the ψ direction [1].

3 Method

As previously mentioned, the aim of this study is to investigate how different parameters related to the diagonal gasket groove affect the mechanical and thermal performance of the heat exchanger. In order to do this, the analysis is performed in three crucial steps. These steps involve generation of the geometry with regards to the chosen parameters, forming simulation of the plates and a gasket analysis. After the gasket analysis, the results regarding each parameter is compared with respect to different values. The outline of the method as a whole can be seen in figure 12.

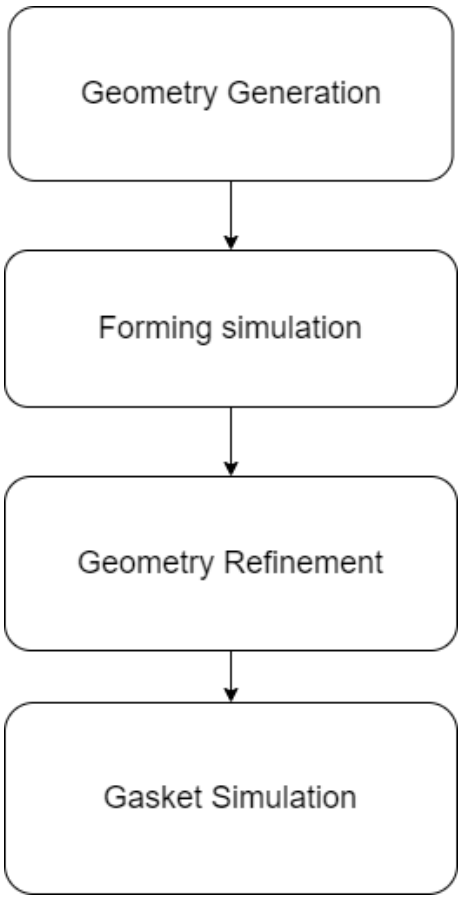

Figure 12: *Flow chart of the method outline*

3.1 Geometry generation

In order to generate each geometry, the first step is to decide on which parameters that are of interest. When the parameters to be analyzed are decided the geometrical limitations have to be evaluated. Each parameter involves up to five different numerical values with increments varying depending on how sensible the parameter is to change.

The parameters that are tested include the following and are described in section 3.1.1,

section 3.1.2 and section 3.1.3:

- Half plane width
- Flank Angles
- Pitch

After discussions with different designers at Alfa Laval, the conclusion is that these parameters will most likely have the highest impacts on the Mechanical and thermal performance of the heat exchanger. The parameters are also tested for two different rubber compounds, namely the EPDM and NBRP compounds.

3.1.1 Half plane width

The half plane width can be seen in figure 13. For this parameter there are no clear geometrical constraints and the parameter could essentially be changed freely.

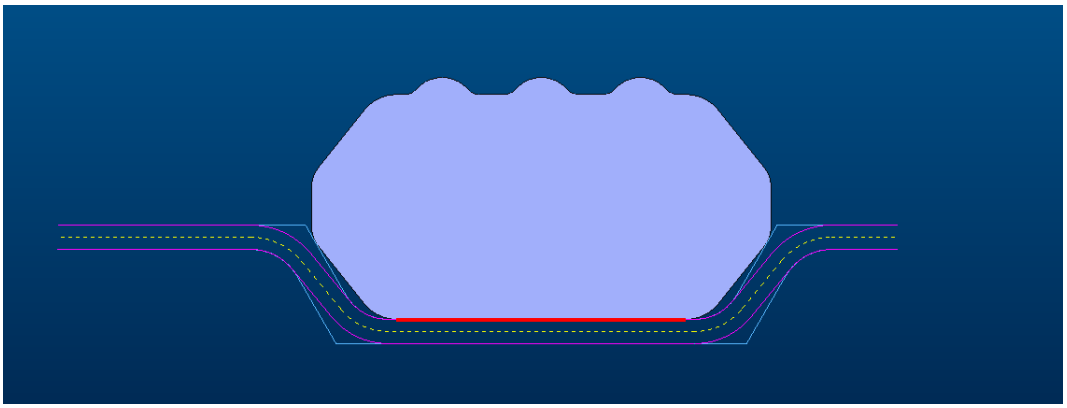

Figure 13: *Half plane width (HPW) illustrated as the red line distance*

3.1.2 Flank angles

The flank angles are illustrated in figure 14. From the figure it can be seen that there are two types of flank angles, one associated with the tool and one associated with the plate. Changing the flank angle associated with the tool subsequently affects the angle associated with the plate. The tool flank angle is the one that is changed during the geometry generation and the actual values of the plate flank angle may vary from the tool flank angles. The figure may be somewhat misleading. The way that the flank angle has been measured in this thesis is from the horizontal plane and not vertical as shown. This means that the tool flank angle in this particular case would be 60°.

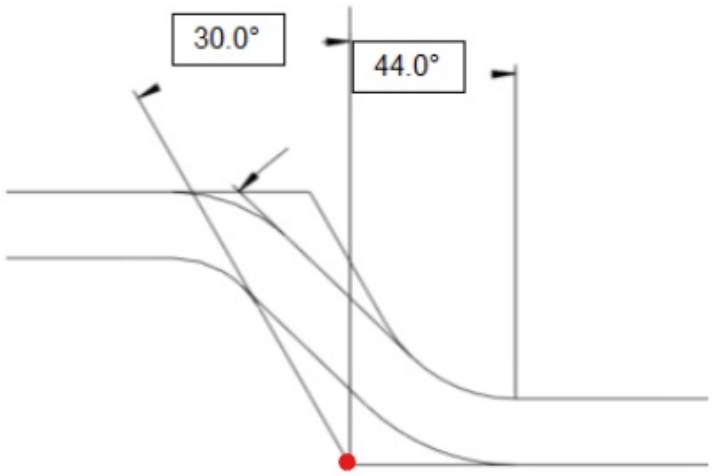

Figure 14: *Flank angles for the tool and plate, illustrated as cross section of the diagonal groove*

The flank angle is changed so that the distance between the stamp and die in the flanks is kept constant. The red point marked in figure 14 is fixed so that the half plane width will not be affected by different values of the flank angle. The parameter has been found to be limited by an upper maximum value of 90°. The lower bound is found to be 0°.

3.1.3 Pitch

The pitch can be seen in figure 15. It is defined as the distance between the two black lines, essentially the distance between the beams radiating from the diagonal groove. The beam widths are kept constant for all values of the pitch, meaning that the pitch is solely affected by increasing the distance between the beams.

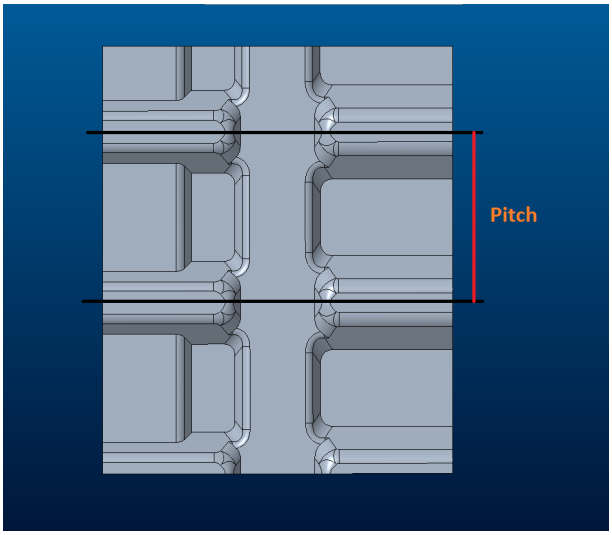

Figure 15: *Pitch illustrated on one of the tools*

The parameter is constrained such that it cannot be smaller than half the beam width since it would result in the beams interfering with each other, no obvious upper limit exists for the pitch.

3.2 Gasket parameters

The parameters of the gasket are changed so that a constant filling ratio is kept since a varying filling ratio can otherwise have larger impacts on the results than the analyzed parameters. When changing the gasket parameters, the goal is to follow the plate parameters. For instance, if the half plane width of the plate is changed, then the corresponding width of the gasket is changed so that the filling ratio is kept constant. In that way, it is clear which parameter actually affects the results.

With these parameters, the tools that are later used in the forming simulation can be generated in the software Creo. The geometry used in the forming simulation consists of a stamp, die and a blank sheet, as illustrated in figure 16. During that simulation, the plate geometries can be created. With the plate geometries created, the gasket geometry is added allowing for the final gasket analysis to be conducted. The forming- and gasket simulation processes are described in detail in section 4 and section 5.

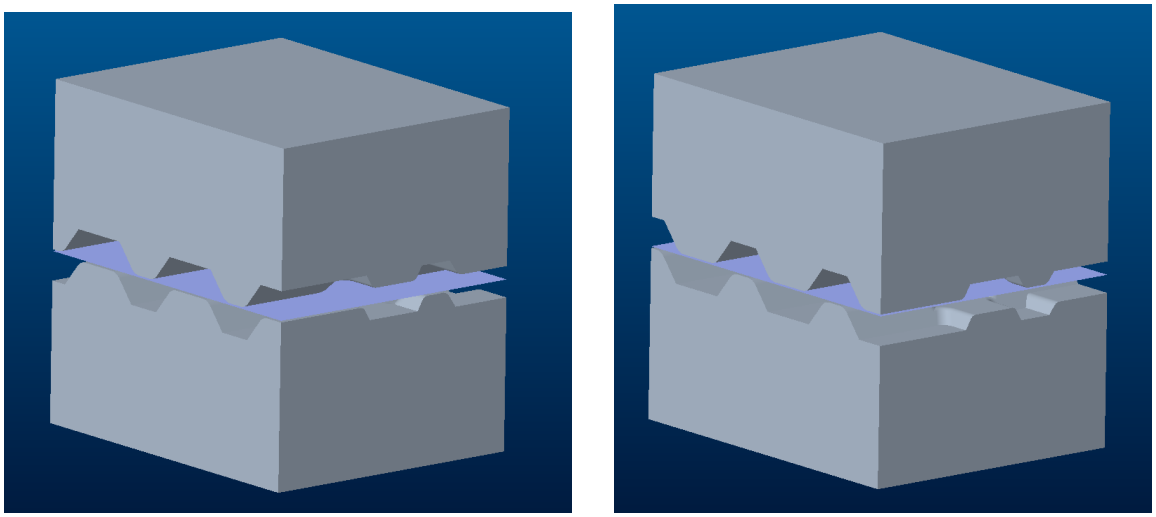

(a) (b)

Figure 16: *Forming tools for the closed side (figure a) and open side (figure b) of the diagonal groove*

4 Forming Simulation

The sheet metal forming simulation is conducted in LS-Dyna which utilizes an explicit method to solve the differential equations. For each geometry, a CAD-model of a stamp and a die is created. The tools together with a blank are pre-processed in Dynaform. When the correct contact relations and material models are added the model is solved using a standardized LS-Dyna solver.

4.1 Pre-processing

The tools that where generated in the geometry generation are exported together with a blank to be pre-processed. The pre-processing is done in Dynaform and includes generation of the mesh for the geometry, defining the materials and material models and establishing the boundary conditions. The method that is used is a standardized method used in Alfa Laval. The method is well tested, which is why no verification has been conducted and no modifications are made.

4.2 Meshing

The meshing is done according to the standardized sizing rules used at Alfa Laval. For the blank, the meshing parameters that can be seen in table 1 is used which generates a mesh according to figure 17.

Table 1: *Meshing parameters for the blank during forming simulation*

Maximum size	0.385 mm
Minimum size	0.385 mm
Chordal deviation	0.01 mm
Angle	10 degrees
Gap tolerance	0.5 mm

The maximum and minimum size of the mesh are the parameters that are geometry dependent and are chosen according to the following formula:

$$Max/min - size = \frac{Pressingdepth}{10} \tag{43}$$

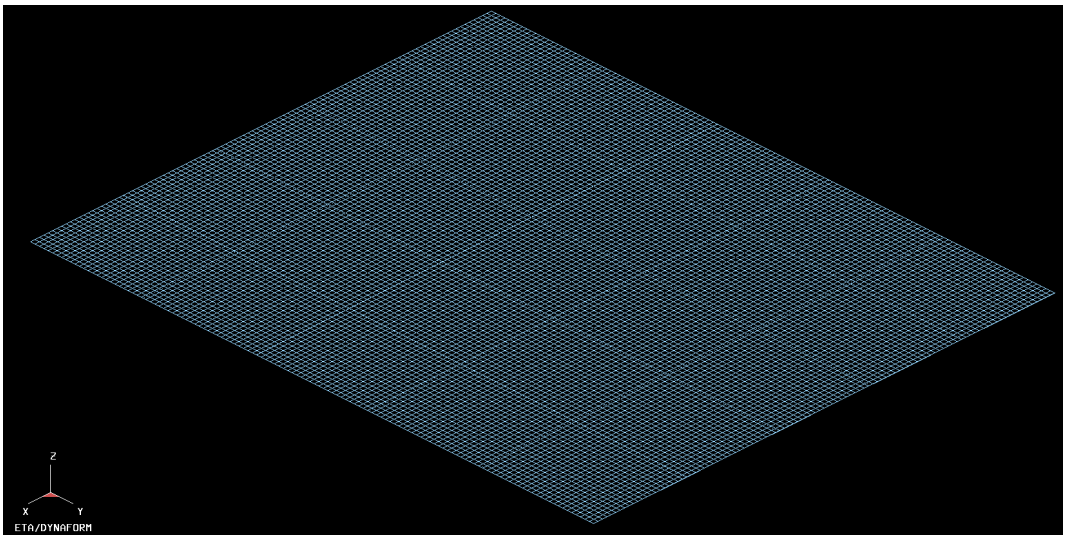

Figure 17: *Illustration of the blank mesh with standard settings*

When meshing the tools, a different set of standardized parameters are used according to table 2.

Table 2: *Standard meshing parameters for the tool*

Maximum size	4 mm
Minimum size	0.01 mm
Chordal deviation	0.01 mm
Angle	10 degrees
Gap tolerance	0.05 mm

The mesh for the die can be seen in figure 18. Here it can be seen that the mesh around the radii and flanks is finer compared to the flat surfaces.

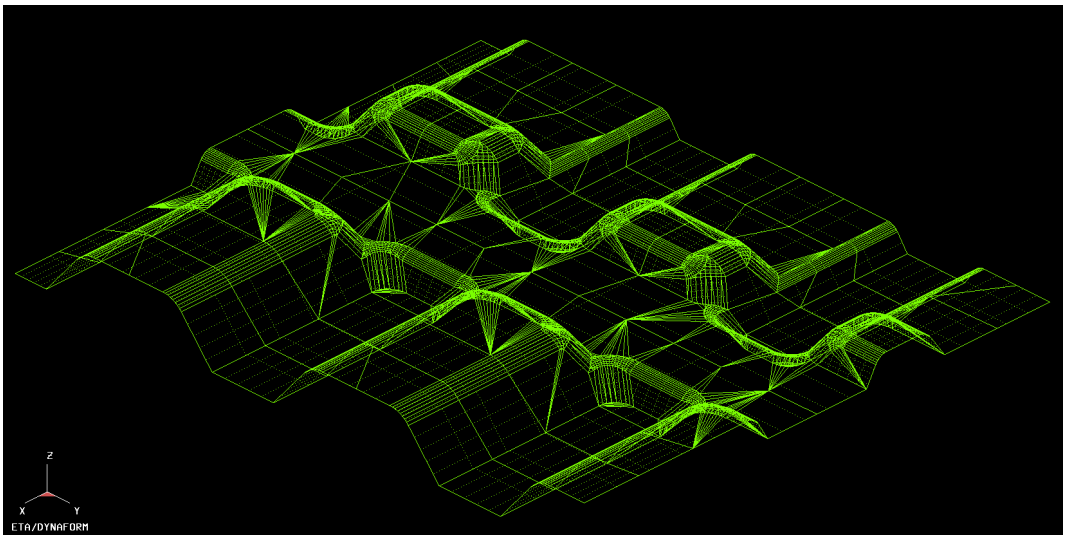

Figure 18: *Illustration of the die mesh with standard tool parameters*

4.3 Boundary conditions

Boundary conditions are required for both the blank and for the tools. The boundary conditions for the blank includes locking the outer nodes in their perpendicular directions. The nodes that are aligned with the x-direction are locked from displacing in the y-direction. The nodes aligned with the y-direction are locked from displacing in the x-direction.

The tools, the die and stamp are given a coefficient of friction of 0.2, which is the standard value used at Alfa Laval. The die is locked in movement while the stamp is subject to a motion curve as can be seen in figure 19.

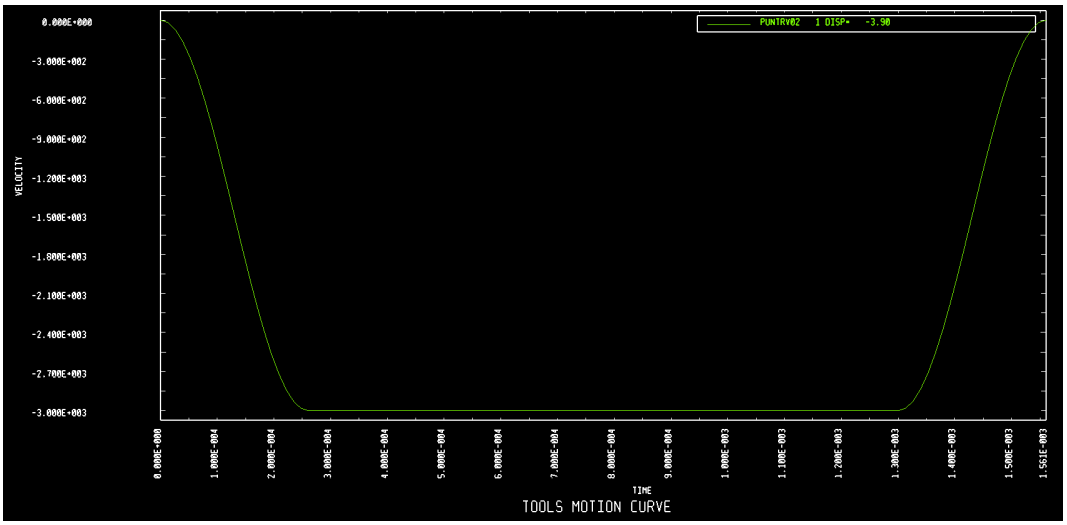

Figure 19: *Motion curve for the stamp, units of velocity is XX and of time is seconds*

The tools are chosen to displace until the final distance between the stamp and die becomes 0.5 mm, corresponding to the plate thickness. The material model used is "Material type 36" that is more thoroughly explained in section 2.11. The contact formulation is also changed to be adapted to stainless steel.

4.4 Solution and post-processing

The numerical simulations are performed using a Alfa-Laval standard solver in LS-Dyna. This solver is based on an explicit method of solving numerical equations that is explained in section 2.9. The solution files can then be post-processed in LS-PrePost where the results for the initial geometry are shown in figure 20. When the solution is completed, the solver solution files can be remade into IGES-files using hypermesh. IGES is a file format that allows for exchange of information between different CAD software's. These files are then trimmed such that the length of the model becomes one pitch. The model is then also adapted for the periodic boundary conditions, that are discussed in section 5.3.

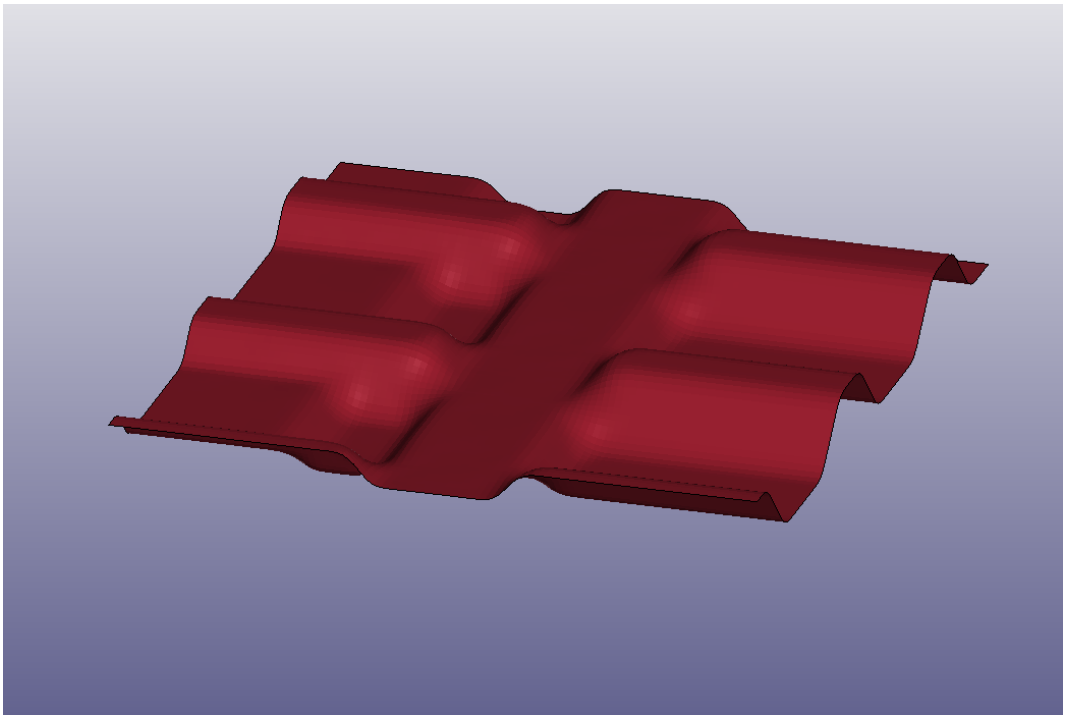

Figure 20: *Pressed plate for the initial configuration*

4.5 Final geometry

The forming simulation results in an upper and a lower plate. These are then trimmed to represent a section corresponding to one pitch. The plates were then assembled together with a gasket to produce a geometry as the one seen in figure 21. This geometry then forms the basis for the gasket simulation that is described in section 5.

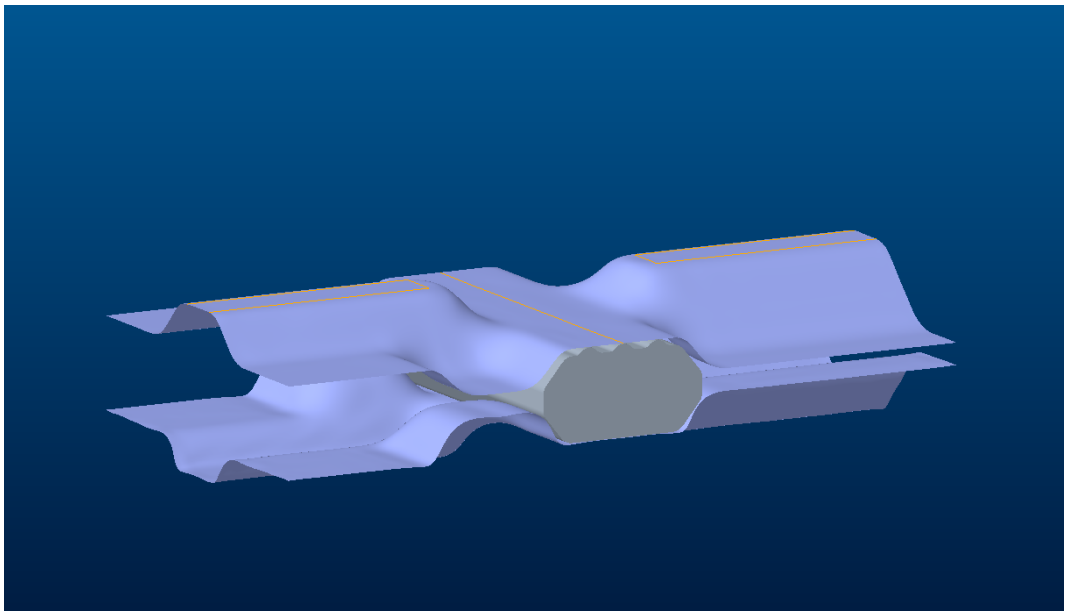

Figure 21: *Gasket simulation geometry from the forming simulations*

The top plate of the geometry represents a cross-section of the open side of the diagonal groove while the bottom plate represents the closed side (see figure 2 for reference) and together they form a small section of two plates mounted to each other with a gasket in between them.

5 Gasket Simulation

The gasket analysis is performed in Ansys static structural. As previously described in section 4.4, the files from the forming simulations are converted to cad files where the gasket are then added. After the gasket is added, the assembly is used in the gasket simulation to generate the final results.

5.1 Meshing

The mesh that has been used in this analysis is a standardized mesh with sizings recommended for the plate used in this study as can be seen in figure 22. Previously, a mesh study has been conducted at Alfa Laval that cannot be shown in this thesis due to confidentiality.

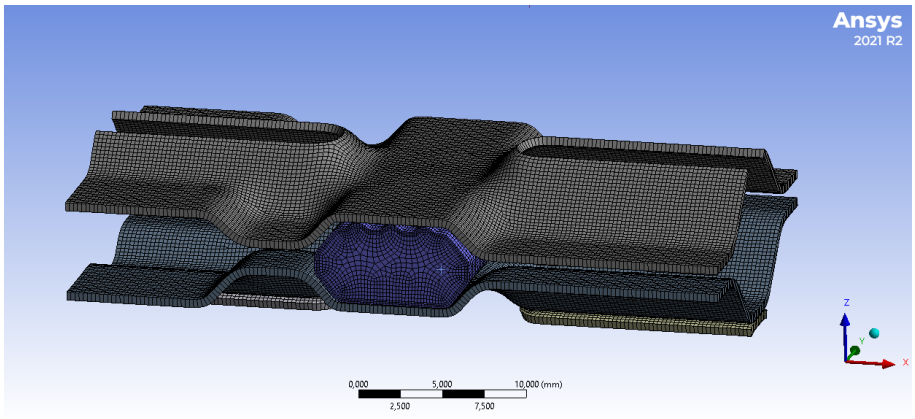

Figure 22: *Full figure of the mesh illustrated on the initial geometry*

The most important meshing parameters for this particular thesis are the ones associated with the gasket. The gasket is meshed with a hex-dominant method. The method creates a mesh that is predominantly made of hedral elements, but allows for some tetrahedrons as can be seen in figure 23 (b). The mesh includes edge sizing and 3 inflation layers that are then swept across the entire gasket body. These are shown in figure 23.

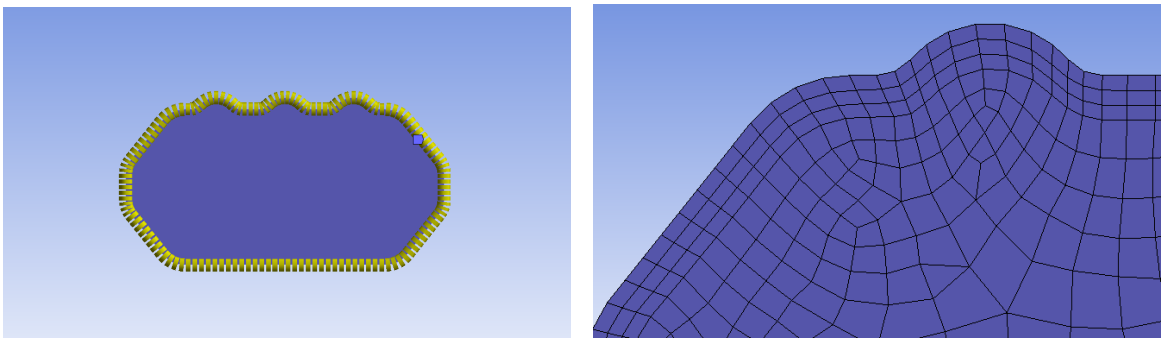

(a) (b)

Figure 23: *Detailed illustrations of the gasket mesh. Subfigure (a) shows the edge sizing location and subfigure (b) shows the inflation layers.*

An alternative to this method would be to use tetrahedrons instead of hedrons. This has, however, not been tested in this thesis. In the mesh study, the difference between using tetrahedrons and hedrons was minimal.

5.2 Contact settings

A modified contact formulation had to be made between the plates and the gasket. The contacts between plates and between plates and gaskets was set to frictional with a coefficient of friction according to Alfa Laval's guidelines. The Coulomb friction model was the one that was used throughout this analysis and is described in section 2.8. Regarding the contact formulation, a pure penalty formulation was used as is described in section 2.7.

5.3 Boundary conditions

The most significant boundary condition for this model is the periodic boundary condition between the *"high_plate_bound"* and *"low_plate_bound"* shown in figure 24.

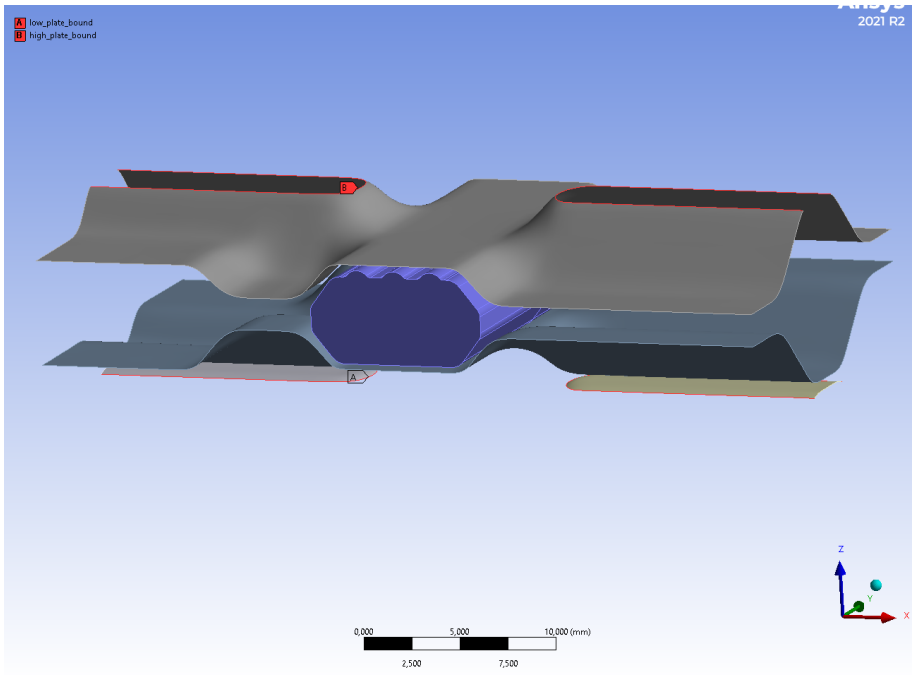

Figure 24: *Edges with periodic boundary conditions*

The condition is that the high and low plate boundaries always maintain exactly the same shape during loading but that they are relatively displaced in the z-direction. The conditions that shall be fulfilled between every node on the low boundary and it's corresponding node on the high boundary is that they shall be coupled meaning that the x and y displacements are the same. The corresponding nodes on the high and low plate boundaries are relatively displaced in the z direction as illustrated in figure 25. The relative displacement during a plate compression simulation is negative but for easier illustration it appears to be positive in the figure.

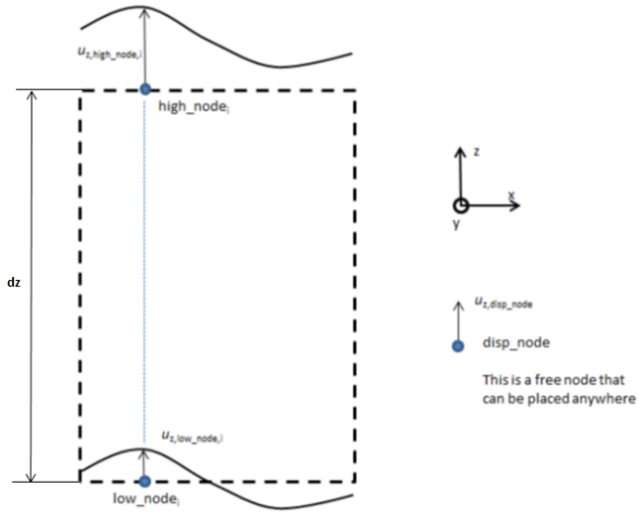

Figure 25: *Illustration of the periodic boundary condition*

This essentially means that the relative displacement from the corresponding nodes is given by the following formula:

$$u_{zH} - u_{zL} = u_{zD} \tag{44}$$

Where u_{zH} and u_{zL} define the displacement of the corresponding nodes on the high and low boundaries and u_{zD} is the user defined displacement.

Apart from the periodic boundary conditions there are also some general constraints that are applied to other regions of the geometry. The first ones are on the plates located on the outer edges of the gasket and plates in the y-direction seen in figure 26. The regions "*symm_plate_bound*" and "*symm_gasket_bound*" are constrained from displacement in the y-direction as well as from rotation around the z- and x-axis.

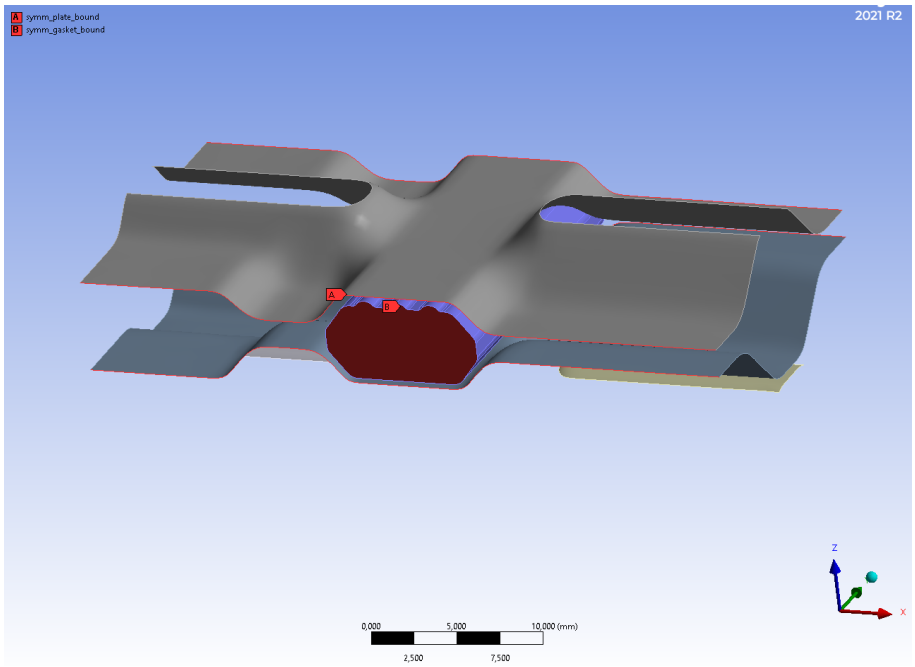

Figure 26: *Y-direction end points for the initial geometry*

Finally there is a similar boundary conditions for the inner and outer bounds of the plates shown in figure 27. The boundaries are constrained from displacing in the x-direction as well as from rotating about the z- and y-axis.

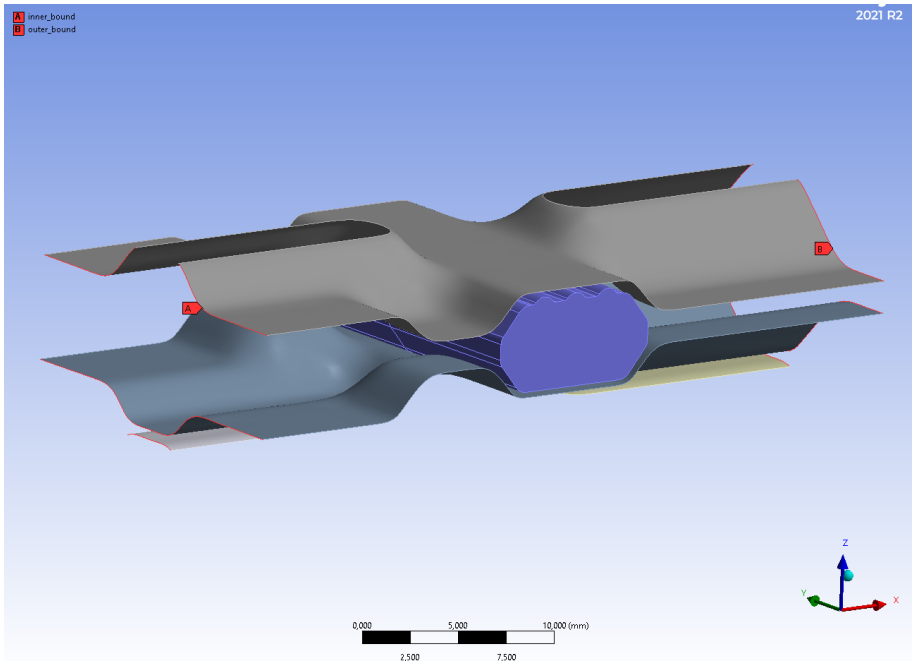

Figure 27: *Inner and outer boundaries of the plates.*

5.4 Solver settings

Since this is a non-linear problem, a non-linear solution algorithm has to be used. The algorithm that is used is the non-symmetrical Newton-Raphson scheme. The Newton-Raphson scheme is described in section 2.6.1. The simulation can be described in two parts, mainly the compression phase and the fluid pressure penetration phase. The compression phase is divided into three steps where the plates are compressed until the free channel height is obtained. The first step includes 70 % of the total compression. In the second step the plates are compressed to 90 % of the total compression and in the final step the remaining displacement is added. If there are difficulties with numerical convergence, another step could be added in order to compress the plates in smaller increments. After the compression phase, the fluid pressure is added. The pressure is ramped up from zero and raised until the leakage pressure is obtained, as discussed next.

5.5 Leakage pressure

The fluid pressure is applied during the final load-step of the solution. The leakage pressure is determined as the pressure required to penetrate across the gasket surface. The fluid pressure is applied from the distribution surface of the geometry and ramped up from zero to a maximum value of 10 MPa. As the analysis approaches the leakage pressure, the solution becomes increasingly unstable. When the fluid pressure finally overcomes the contact pressure and penetrates the gasket surface, the state of the problem changes into one that no longer can be described with an implicit FE-method, as is used here. This in turn leads to the simulation crashing, whereby the pressure for the last sub step before the crash is extracted.

The method of determining the leakage pressure is frequently used at Alfa Laval. Comparisons with physical tests in the past have shown that the numerical value of the leakage pressure deviates from the actual leakage pressures observed. However, when comparing different geometries, the method has proven very effective in determining which geometry that will be the first to leak which makes it well suited for a comparing analysis such as the one conducted in this thesis. It is important to note that each analysis has to be thoroughly controlled as to whether the simulation crashed due to the fluid pressure penetration or if it perhaps was due to other reasons. This was done visually after each simulation. The pressure can be seen to have penetrated across the entire surface of the gasket, and it can thereby be concluded that leakage has occurred.

6 Results

The results will be presented for each parameter separately. In this section the sensitivity for each result will be included while the more detailed results can be found in the appendix. Due to confidentiality, the results will be presented as deviations from the initial value. The results will be presented for the NBRP and EPDM rubber compound separately. The results include fluid pressure and contact pressure for the gasket across different sections.

6.1 Measurement of results

The results are measured on four regions of the gasket. The regions can be seen in figure 28 and figure 29. The main reason for measuring the results in this way is to avoid the effects of node singularities that might occur. If for instance the geometries were compared with respect to maximum values, then it is hard to know whether the maximum value comes from a node singularity or if it actually comes from the geometry itself.

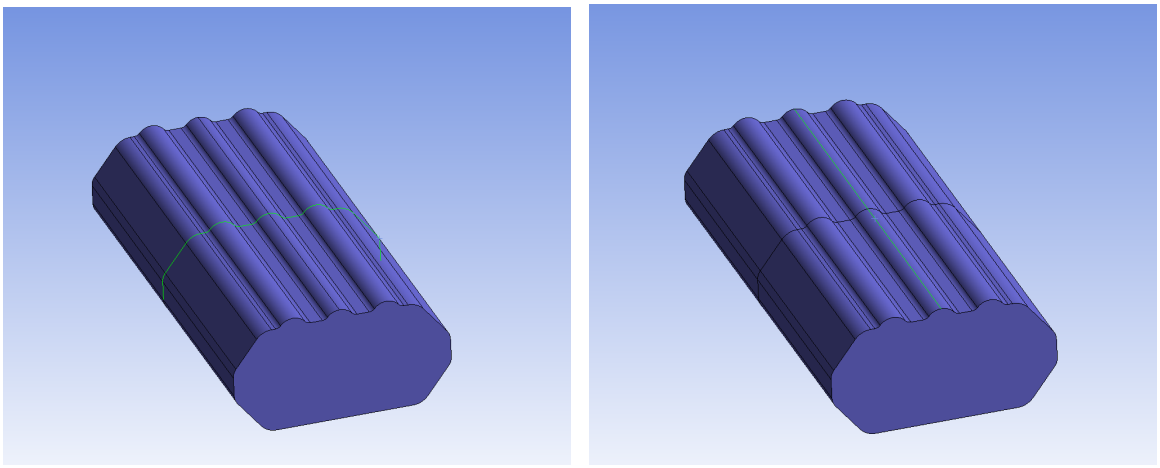

Figure 28: *Measurement region "Gasket Top X-axis" to the left and "Gasket Top Y-axis" to the left shown as green lines*

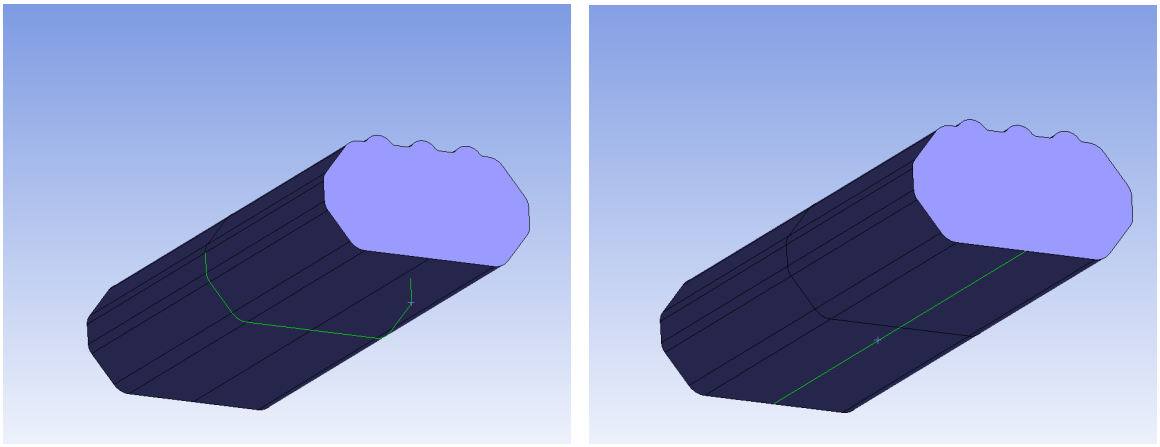

Figure 29: *Measurement region "Gasket Bot X-axis" to the left and "Gasket Bot Y-axis" to the left shown as green lines*

The leakage pressure can be measured in two ways. One way is to linearly ramp the fluid pressure to a very high magnitude and see where the simulation crashes. This indicates that the fluid pressure has passed through the gasket and that there is leakage. The other way is to for a constant maximum fluid pressure measure how far into the gasket the fluid reaches. The second way can be problematic when different geometries are compared since there can be geometrical factors such as the rib's relative position on the gasket that affect the results.

6.2 Results for the initial geometry

The results for the initial geometry are presented in figure 30 and figure 31. These results are presented so that the reader can get a picture of the general behaviour of the gasket during compression and fluid pressure.

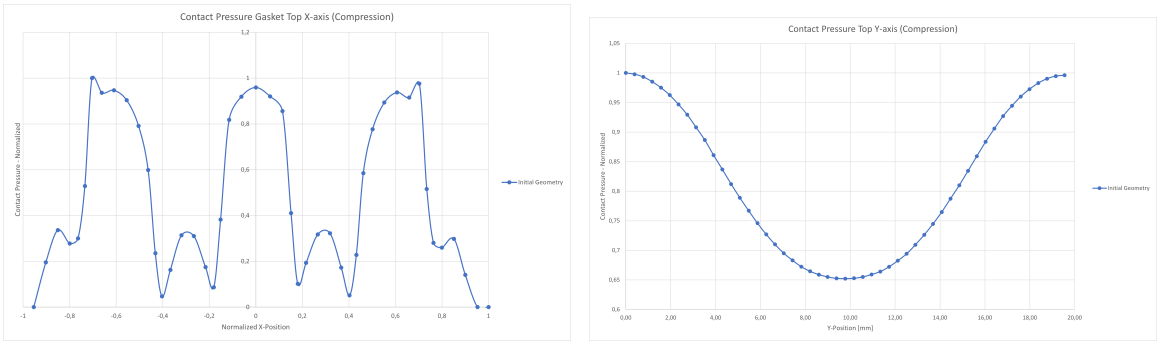

Figure 30: *Contact pressure for the gasket top lines. X-axis shown to the left and Y-axis shown to the right*

For the bottom side, the result in figure 31 were obtained. The general behaviour of the

results is similar for all parameters that where examined during this thesis.

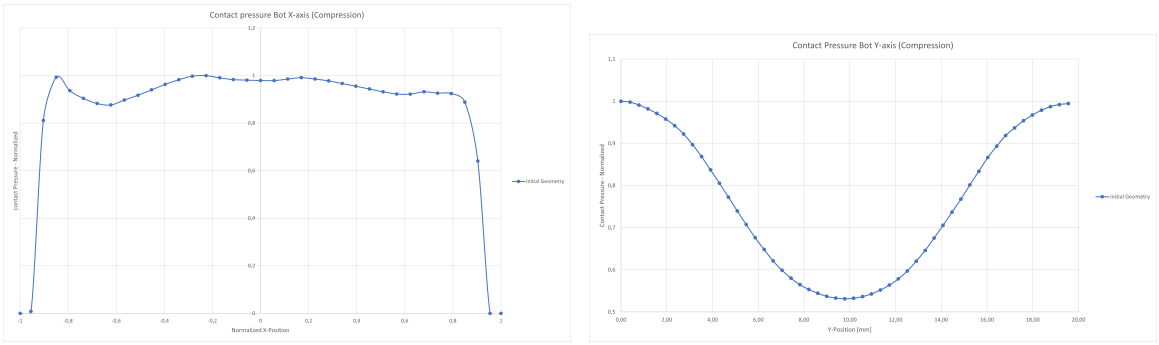

Figure 31: *Contact pressure for the gasket bot lines. X-axis shown to the left and Y-axis shown to the right, cf. figure 29*

6.3 Half plane width

The results presented in this section are related to the half plane width. For this parameter, five data points are used where the length of the half plane width (HPW) is changed with increments of five percent. Some extreme values are also tested and the results of these studies are included in the appendix.

After the second time step, i.e. after the compression of the plates, the results shown in table 3 are obtained.

Table 3: *Average contact pressure for different values of HPW after the second time step.*

Half plane width contact pressure results				
Parameter	Deviations from the initial geometry - EPDM compound			
	Top X-axis	Top Y-axis	Bot X-axis	Bot Y-axis
HPW -5%	-3.21 %	+1.32 %	+2.01 %	+2.88 %
HPW -10%	-2.30 %	-0.96 %	+1.97 %	+2.04 %
HPW +5%	-1.35 %	-1.05 %	-2.01 %	-2.37 %
HPW +10%	-0.79 %	-1.81 %	-3.94 %	-3.97 %
	Deviation from initial geometry - NBRP Compound			
HPW -5%	-3.85 %	-1.66 %	-1.23 %	-0.65 %
HPW -10%	-5.18 %	-2.71 %	-0.76 %	-1.35 %
HPW +5%	-0.09 %	-0.25 %	-1.23 %	-1.23 %
HPW +10%	+1.62 %	+0.03 %	-1.99 %	-1.23 %

After the third time step when the fluid pressure was added, the results shown in table 4 are obtained.

Table 4: *Average contact pressure for different values of HPW after the third time step.*

Half plane width contact pressure results				
Parameter	Deviations from the initial geometry - EPDM compound			
	Top X-axis	Top Y-axis	Bot X-axis	Bot Y-axis
HPW -5%	-1.14 %	+0.96 %	+1.81 %	+3.03 %
HPW -10%	+5.02 %	+1.48%	+0.80%	+5.21 %
HPW +5%	-3.63 %	-1.59 %	-2.02 %	-2.95 %
HPW +10%	-4,14 %	-3,34 %	-4,18 %	-5,87 %
	Deviation from the initial geometry - NBRP compound			
HPW -5%	+0.66 %	-0.24 %	+0.54 %	+1.55 %
HPW -10%	+2.80 %	-0.20 %	+3.02 %	+2.33 %
HPW +5%	-3.57 %	-0.78 %	-1.16 %	-1.98 %
HPW +10%	-6.31 %	-2.44 %	-3.83 %	-4.67 %

The leakage pressures NBRP and EPDM rubber compounds are shown respectively in figure 32 and figure 33. The values are normalized for both the half plane width and the leakage pressures where the values for the initial geometry is represented as 1.

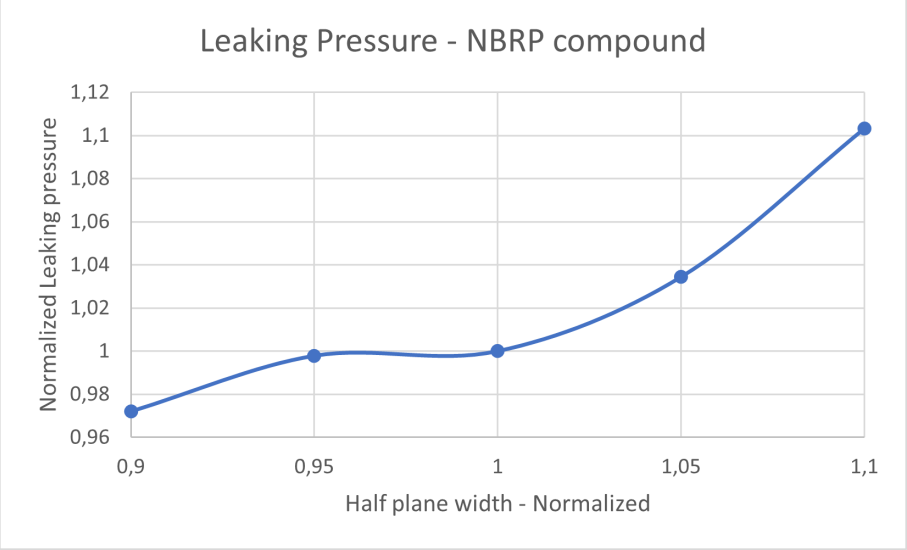

Figure 32: *Leakage pressure for different half plane width values with NBRP rubber compound*

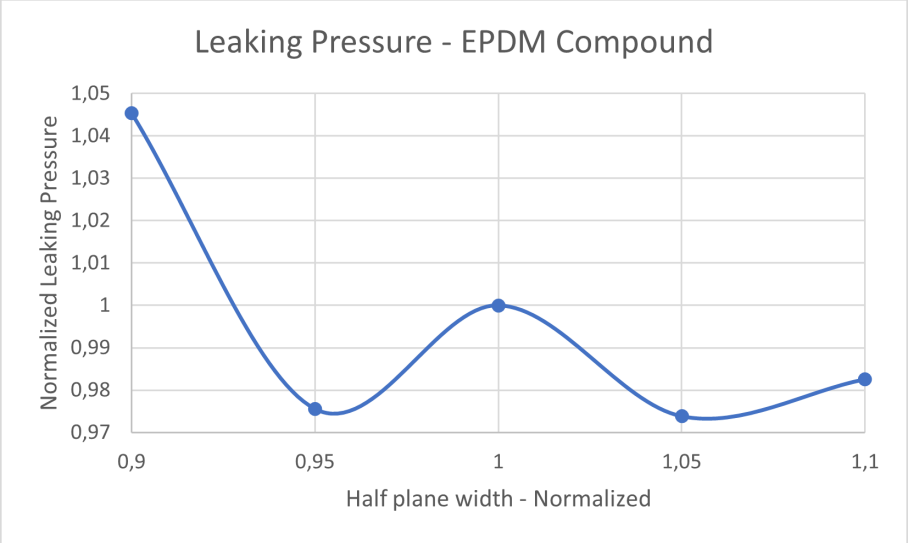

Figure 33: *Leakage pressure for different half plane width values with EPDM rubber compound*

Table 5: *Volume-Opening ratios for different parameters*

Parameter	Volume-Opening ratio
Initial geometry	14.48
HPW +5%	13.87
HPW +10%	13.26
HPW -5%	15.09
HPW -10%	15.70

The strains shown in figure 34 are normalized by 1 as the maximum value. In the figure, the threshold strain for when the stiffness of the material model starts to increase is marked with a black line. The reader is also referred to figure 11 for the case of biaxial loading.

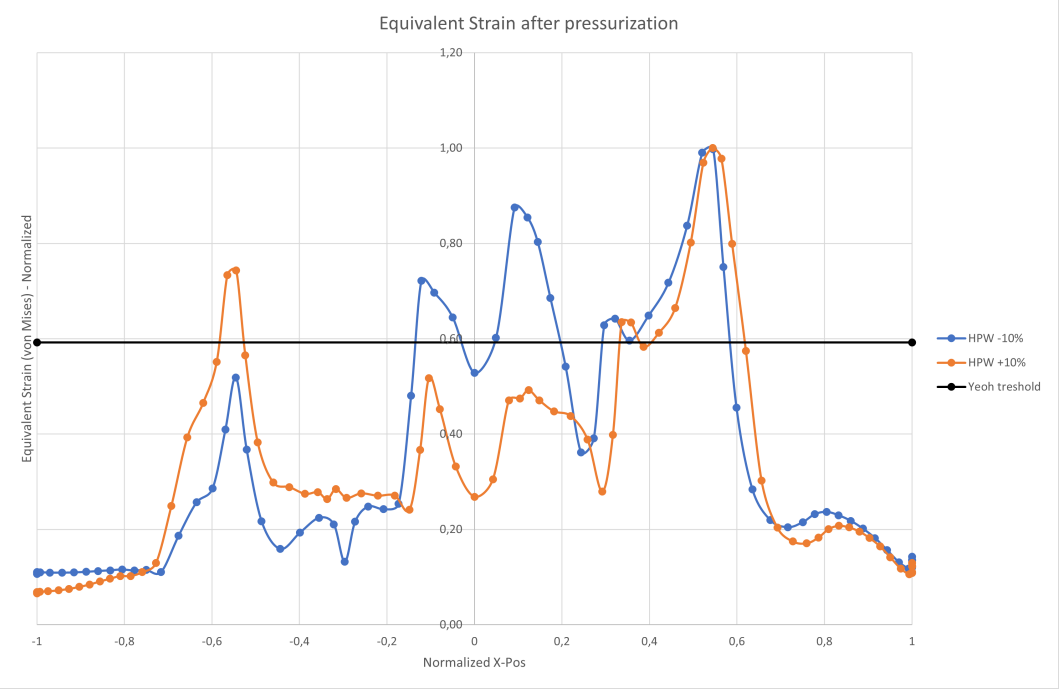

Figure 34: *Strains obtained after the pressurization, shown for extreme values of HPW with the NBRP rubber compound*

6.4 Flank angle

The results presented in this section are associated with the flank angle of the tools. The gasket geometry is changed in the same way as the groove area geometry so that the filling ratio is kept at a constant value. Diagrams associated with the results can be found in the appendix. As previously mentioned, the parameters are changed with the tools as basis. The relationship between the tool flank angle and the plate flank angle can be found in table 6.

Table 6: *Relationship between tool and plate flank angles*

Tool flank angle	Plate flank angle
40°	35.8°
50°	43.7°
60°	50.5°
80°	55.6°

After the compression load step, that includes displacement of the plates, the results in table 7 and table 8 are obtained.

Table 7: *Average contact pressure for different values of the tool flank angles (FA)after the second time step.*

Flank angle contact pressure results				
Parameter	Deviations from the initial geometry - EPDM compound			
	Top X-axis	Top Y-axis	Bot X-axis	Bot Y-axis
FA 40°	-3.203 %	-2.007 %	-5.231 %	-2.586 %
FA 50°	-3.434 %	-0.525 %	+2.083 %	-0.687 %
FA 80°	-3.385 %	-2.795 %	-1.032 %	-3.241 %
	Deviation from the initial geometry - NBRP compound			
FA 40°	-0.405%	+0.048%	-0.441%	-0.041%
FA 50°	-1.481%	-0.726%	1.849%	-0.664%
FA 80°	-4.679%	-4.022%	-2.336%	-4.741%

Table 8: *Average contact pressure for different values of the tool flank angles (FA) after the third time step.*

Flank angle contact pressure results				
Parameter	Deviations from the initial geometry - EPDM compound			
	Top X-axis	Top Y-axis	Bot X-axis	Bot Y-axis
FA 40°	-5.213 %	-3.994 %	-5.059 %	-5.220 %
FA 50°	-0.937 %	-0.773 %	-1.485 %	-0.783 %
FA 80°	-0.687 %	-2.418 %	-3.647 %	-2.128 %
	Deviation from the initial geometry - NBRP compound			
FA 40°	-4.147 %	-2.098 %	-3.578 %	-3.414 %
FA 50°	-1.766 %	-1.450%	-2.404 %	-1.431 %
FA 80°	-2.828 %	-2.109 %	-0.178 %	-1.922 %

The leakage pressures that are recorded can be seen in figure 36 and figure 35 where the absolute values have been normalized due to confidentiality. The values for the leakage pressure have been normalized in a way that 1 represents the leakage pressure for the initial geometry.

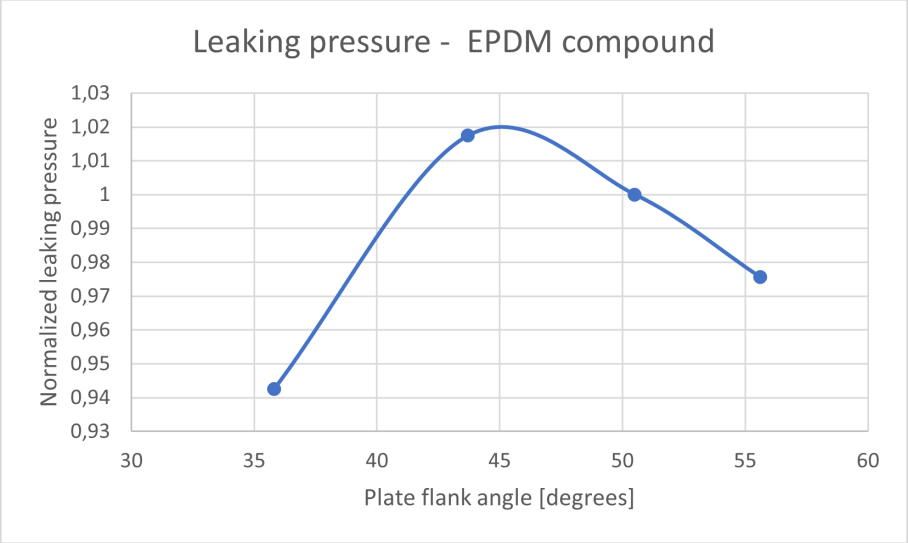

Figure 35: *Normalized Leakage pressure for the EPDM rubber compound*

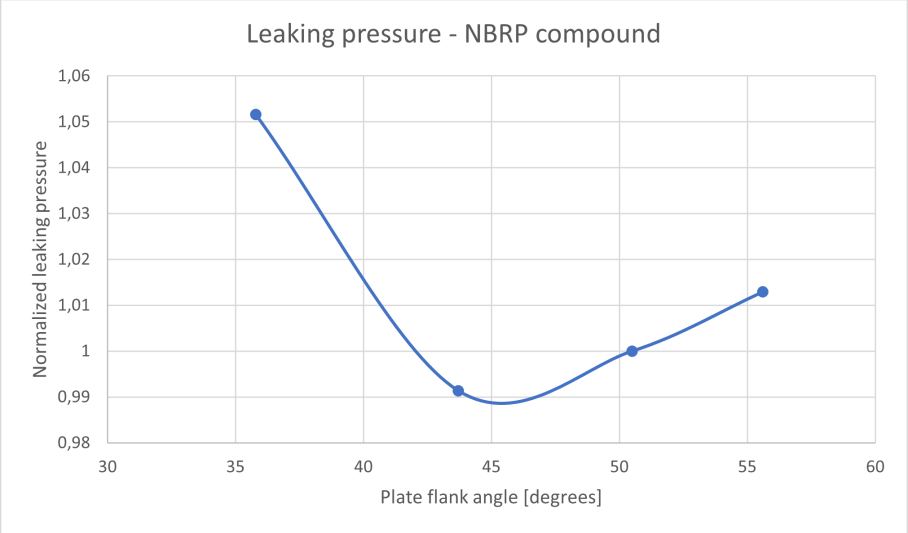

Figure 36: *Normalized Leakage pressure for the EPDM rubber compound*

Table 9: *Volume-Opening ratios for different parameters*

Parameter	Volume-Opening ratio
FA 60°(Initial)	14.48
FA 40°	15.71
FA 50°	14.91
FA 80°	14.25

6.5 Pitch

The results presented in this sub section are related to the pitch. The average contact pressures along the different lines illustrated in figure 28 and figure 29 are shown in table 10 and table 11 as deviations from the initial values. The results are shown separately for gaskets with EPDM and NBRP rubber compounds.

Table 10: *Average contact pressure values for variations of the pitch after the compression load step*

Pitch contact pressure results				
Parameter	Deviations from the initial geometry - EPDM compound			
	Top X-axis	Top Y-axis	Bot X-axis	Bot Y-axis
Pitch -10%	+1.91%	+2.23%	+6.72%	+3.77%
Pitch +10%	-4.13%	+1.03%	-2.91%	-0.32%
Pitch +20%	-7.96%	-4.78%	-5.61%	-5.12%
Pitch +30%	-6.58%	-3.32%	-4.01%	-4.26%
	Deviation from the initial geometry - NBRP compound			
Pitch -10%	+5.11%	+2.69%	+10.85%	+4.30%
Pitch +10%	-5.99%	-1.01%	-4.50%	-2.47%
Pitch +20%	-6.06%	-2.86%	-3.05%	-3.57%
Pitch +30%	-8.85%	-5.51%	-5.56%	-7.21%

Table 11: *Average contact pressure values for variations of the pitch after the compression and pressurization load step*

Pitch contact pressure results				
Parameter	Deviations from the initial geometry - EPDM compound			
	Top X-axis	Top Y-axis	Bot X-axis	Bot Y-axis
Pitch -10%	+5.17%	+3.69%	+7.24%	+6.12%
Pitch +10%	0.00%	+2.74%	-0.07%	+2.12%
Pitch +20%	-0.30%	+0.14%	-0.18%	+0.80%
Pitch +30%	-0.40%	-0.40%	+0.45%	-0.07%
	Deviation from the initial geometry - NBRP compound			
Pitch -10%	+5.53%	+11.03%	+7.13%	+5.88%
Pitch +10%	-1.49%	7.72%	-1.60%	0.23%
Pitch +20%	-3.19%	3.25%	-3.14%	-2.11%
Pitch +30%	-3.80%	2.56%	-2.85%	-3.19%

Figure 37 and figure 38 show the recorded leakage pressures for the NBRP and EPDM compounds, respectively. The values are normalized due to confidentiality reasons.

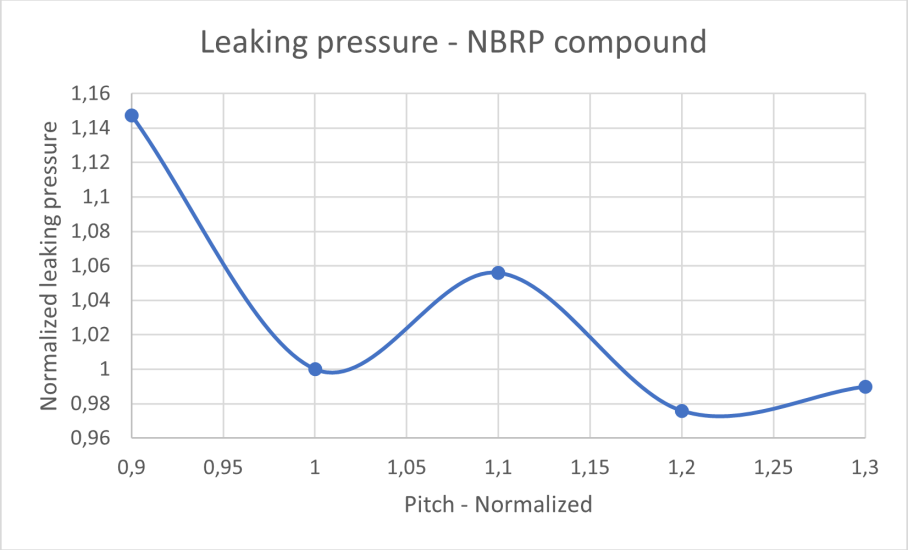

Figure 37: *Leakage pressure for different pitch values with NBRP rubber compound*

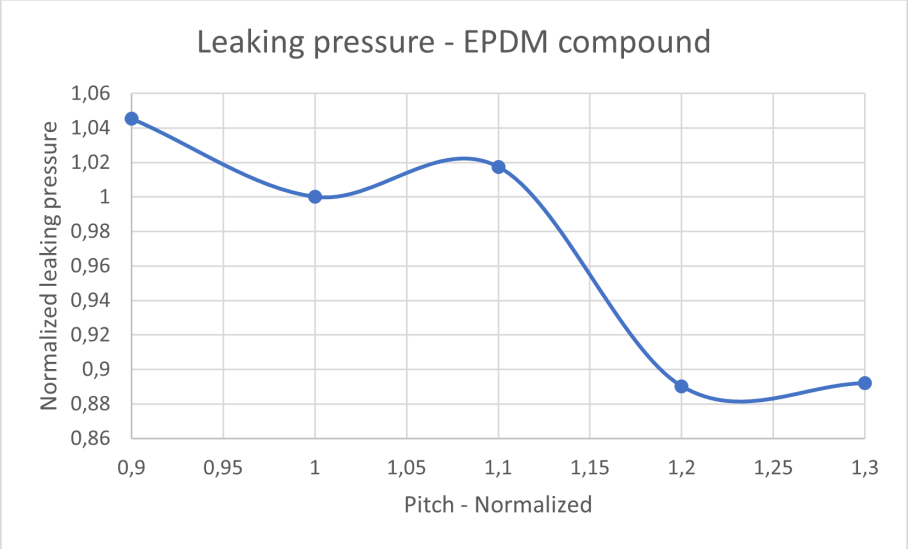

Figure 38: *Leakage pressure for different pitch values with EPDM rubber compound*

The volume opening ratios are shown for the different geometries which are tested in table 12.

Table 12: *Volume-Opening ratios for different parameters*

Parameter	Volume-opening ratio
Initial Geometry	14.48
Pitch -10%	17.95
Pitch +10%	12.45
Pitch +20%	11.15
Pitch +30%	10.24

7 Discussion

In this section, the results will be addressed and some possible explanations will be given. Apart from the results, possible sources of error will be discussed and some suggestions on further development will be given.

7.1 Half plane width

When observing the results for the half plane width, a pattern can be seen. Higher values on the half plane width seem to increase the contact pressure between the gaskets and the plates on all the regions of measurement. However, as the fluid pressure is added, the results seem to shift and the smallest plates seem to contribute to the largest contact pressures. When the deviations are considered, it can be seen that the results do not deviate a lot from the initial values which suggests that there is only a small sensitivity with respect to this parameter.

Before conducting the analysis, the hypothesis was that a larger value of the half plane width would result in a lower contact pressure. The reasoning behind this was that a larger width would lead to the plate being more prone to bending which in turn results in a decrease in the contact pressure. The results that were obtained partially contradict this statement, at least when the first load step was considered. Explaining the results can be quite challenging due to the complex nature of the problem.

There are many different factors that most certainly will affect the outcome of the analysis. The first thing that comes to mind is the incompressibility of the gasket. As the half plane width is increased, the gasket width is increased as well in order to preserve the filling ratio from the initial geometry. In turn, when the gasket width is increased, the volume of the gasket increases accordingly. However, the cross section of the opening between the beams radiating from the diagonal groove remains the same since the pitch is kept constant. As the plates are compressed onto the gasket, the compressed volume of the gasket must escape through the opening area since the gasket is incompressible. If a larger half plane width is used the result will be that a larger volume of the gasket must escape through the same opening cross section which in turn could result in a larger contact pressure for larger half plane width values.

When trying to explain the shift in contact pressure between the compression step and pressurization step the strains for the extreme values become particularly interesting. This can be seen in figure 34. The strains recorded for the small gasket are to a larger extent above the threshold for when the material model for the gasket becomes very stiff. This behaviour is particularly visible in the center rib of the gasket seen in figure 34, between the normalized

distance -0.2 and 0.2. For pressurization combined with compression, the loading case is biaxial and the Yeoh model shown in figure 11 at a certain threshold becomes very stiff.

Another factor that was addressed was that a smaller value of the half plane width could result in the plates experiencing plastic strain at an earlier stage. This in turn would dramatically decrease the contact pressure. However, when the results were assessed it could be seen that there was almost no plastic strain observed in any of the tested geometries.

Looking at the results, it can be seen that the deviations are very small. One explanation for this could be that there are several factors which contradict each other. The plate being more prone to bending together with the incompressible nature of the gasket could, when combined, cancel each other out.

The results regarding the leakage pressure were in line with the ones regarding the contact pressure. A wider half plane width resulted in higher leakage pressures. A notable difference was that the results regarding the leakage pressure deviated more from the initial value when compared to the results regarding the contact pressure. It should be noted that a wider gasket results in a larger surface area that needs to be penetrated which can help explain the increased deviations.

When the different rubber compounds are compared, it can be seen that the gasket volume effect tends to decrease. When the EPDM rubber compound was used, the geometries which the HPW was decreased seem to result in an increase of the contact pressure for both the compression load step as well as for the pressure penetration load step. This is contrary to the case when the NBRP compound was used where these effects were only seen for the pressure penetration load step. The EPDM compound is stiffer which makes it less prone to compression. The incompressibility effects that have previously been discussed then decrease and parameters related to the plates play a larger role. Concerning the fluid pressure the effect of changing the rubber compound is dramatic. The geometries that previously generated the highest leakage pressure now instead generate the lowest leakage pressures.

7.2 Flank angles

The results regarding the flank angle are similar to the results regarding the half plane width in that they do not deviate significantly from the initial value. What is interesting with regards to these results is that the initial geometry seems to produce the highest contact pressure of the four samples investigated.

When the results in table 8 are compared to those in table 7, a shift in the deviations can be observed. The values of the higher tool flank angle of 80°seem to approach the initial values while the lower flank angles seem to deviate more from the initial. This could suggest that the contact pressure for the flatter flank angles is more sensitive to added fluid pressure when compared to the higher values of the flank angle.

When trying to understand the effects of the flank angle, one can quickly come to the conclusion that this parameter is even more complex than the half plane width. As the flank angle is changed, the load case of the entire problem changes with it. For larger values of the flank angle, such as 60°and 80°, the loading becomes increasingly biaxial since the x-component of the flank contact forces increases. As has previously been mentioned, the Yeoh material model used in the rubber compound becomes increasingly stiff at a certain strain value when biaxial loading is present which in turn could result in an increased contact pressure. However, as the flank angle is decreased, the volume of the entire gasket increases, resulting in an increase of the volume-opening ratio as can be observed in table 9. This may, in turn, affect the overall contact pressure of the gasket.

Regarding the leakage pressure, the highest values seem to occur for the smallest and largest flank angles although it should be noted that the deviations are very small. There is no clear pattern that can be seen regarding this parameter and there are many possible causes for the deviations. The effect of decreasing the flank angle is that the contact surface becomes larger, thus making the gasket harder to move. When the flank angle becomes larger, the effect could be that the gasket itself becomes stiffer due to its material properties.

When the rubber compounds are compared, the behaviour seems to be the same regarding the contact pressure, although the deviations from the initial value seem to be larger. However, the leakage pressure for the EPDM compound, seen in figure 35, almost seems to be a mirrored image of the curve for the NBRP compound, shown in figure 36. It should be noted that the volume opening ratios for this parameter do deviate a lot from the initial value.

7.3 Pitch

This parameter is different from the half plane width and the flank angle since the gasket geometry is not changed during the analysis. The changes only apply to the plates. For the contact pressure the results show that a larger pitch results in a smaller contact pressure. This behaviour is observed both after the compression step and when the internal pressure is applied. The leakage pressure follows the contact pressure meaning that a larger value on the pitch results in earlier leakage pressures. The effects are most notable when the pitch is decreased. Table 10 and table 11 show large fluctuations of the pitch for contact pressures

related to "*Pitch -10%*".

For this parameter, the volume-opening shown in table 12 is of particular interest. Decreasing the pitch results in large deviations of the volume-opening ratio. Together with the large deviations in contact- and leakage pressures associated with the geometry, this strengthens the claims concerning the effects of incompressibility discussed in section 7.1 and section 7.2. As the pitch increases, the volume opening ratio deviates less for each increase which could explain why the results regarding the larger pitch values do not deviate alot from each other.

Concerning the leakage pressure, the overall behaviour seems to be in compliance with the contact pressure. The results regarding this parameter comply well with the expectations. Apart from the theories presented in the previous sections, another explanation to the leakage pressure decreasing with increased pitch size can be that the larger portions of the gasket are blocked from traversing in the direction of the fluid in the small pitch compared to the larger ones.

When the different rubber compounds are compared for the pitch geometries, a similar behaviour can be seen between the NBRP and EPDM rubber compounds. The main difference is that the deviations seem to be smaller for the EPDM compound. This is reasonable if the incompressibility characteristics of the gaskets are considered. The EPDM rubber compound is stiffer and therefore harder to compress when compared to the NBRP compound and the impact of the changed volume-opening ratio seen in table 12 decreases. Concerning the leakage pressures, the general behaviour seems to be similar, although the smaller values seem to deviate more for the NBRP compound when compared to the EPDM compound. This can be seen in figure 37 and figure 38.

7.4 Sources of error

The problem at hand is a very complex one and there are many different factors that can play a crucial role in the outcome of the analysis. In this section a number of such problems will be presented.

To conduct this analysis, a non-linear FE model was used and just as any other FE-model it will deviate somewhat from the reality. There are several reasons for this. One such reason could be that no transfer of the material history occurs between the forming and gasket simulations. Due to this, effects such as springback and necking are neglected in the analysis.

Another problem is that the coefficient of friction used in the analysis deviates from reality.

The reason for this is convergence issues. This error might impact the gaskets ability to expand on the plate as well as it's ability to traverse across the plate when fluid pressure is added. Both during the forming and gasket simulations, the Coulomb friction model was used. The Coulomb friction model is a very simplified version of the actual frictional behaviour. For the gasket simulations where only static behaviour is considered, the model might be well suited but for the forming simulations where velocity effects are considered, the approximation becomes less accurate. For instance, the Stribeck effect is ignored in this analysis.

The analysis is performed for room temperature conditions. This does not give the complete picture of reality as the operating temperatures deviate a lot from room temperature. Effects such as thermal expansion that most certainly affect the contact pressure are not analyzed. Apart from this, no consideration of the material properties at elevated temperatures is accounted for as it would make the problem more complex.

It should also be noted that this is a perfect state analysis. There are no imperfections on the gasket nor the plate tools before they go into the analysis. In reality, such imperfections do occur and tolerances can play a major part on the outcome of the mechanical performance. Apart from this, the analysis is performed on one plate only and it is not certain that the same results are applicable on other plate designs. It is also only performed on a small part of the diagonal and it is not certain that the same behaviour would be seen on a larger scale.

7.5 Future work

The aim of this thesis covers a very broad scope and there are many more parameters that could be analyzed. Such parameters could for instance be plate radii or parameters related to the beams.

Regarding the parameters that have already been analyzed, real life testing should be performed in order to validate the results. The parameters could also be further analyzed by testing them for different operating temperatures of the heat exchanger. Apart from this the same parameters could also be tested on different plates in order to determine whether similar behaviours can be observed.

Concerning the modelling, a method that allows for the use of higher coefficients of friction should be developed in order to produce more accurate results. The parameters which were tested should also be evaluated from a manufacturing standpoint. For instance, a flank angle of 80°for the tools might be very hard to manufacture.

8 Conclusion

At the start of this project, the main goal was to analyze as many parameters as possible to aid engineers in their design process regarding the diagonal groove. As the thesis progressed, it was found that the results did not reflect the hypothesis and the problem at hand was far more complex than what was initially thought. Consequently, the focus was shifted towards obtaining a better theoretical understanding of the studied parameters. Fewer parameters that were thought to have large effects on the results were thoroughly analyzed with different rubber compounds and plate materials in mind.

Previously, many of the assumptions made regarding the mechanical performance have been based on the plates. For instance, regarding the half plane width, the theory was that a wider plate would decrease in stiffness which in turn would contribute to a lower contact pressure. This might be true, but for small changes on the plate geometry the effects are minimal. In reality the results from this thesis seem to show that changes on the gasket geometry play a much larger role concerning the mechanical performance of the heat exchanger.

The filling ratio, although giving some valuable information, is not on its own a sufficient measure to analyze the relationship between the gasket and the plate. The gasket needs to be analyzed from a volume perspective where its freedom to elongate when compressed is an important factor when mechanical performance is considered.

Apart from this, it should be noted that this is a very complex physical problem where numerous scenarios exist that can dramatically affect the results. The analysis conducted in this thesis is a simplification of the problem and the real use case of the product adds even more complexity in terms of high temperature deviations and imperfections of the geometry. With these things considered, this thesis may still give some very valuable insight into the design effects on the mechanical performance of a heat exchanger.

References

[1] F. Barlat and J. Lian. "Plastic behavior and stretchability of sheet metals. Part I: A yield function for orthotropic sheets under plane stress conditions". In: International Journal of Plasticity 5 (1989), pp. 51–66. DOI: https://doi.org/10.1016/0749-6419(89)90019-3.

[2] Timothy Bui. "Explicit and Implicit Methods In Solving Differential Equations". In: Honors Scholar Theses (2010).

[3] Steen Krenk. Non-linear Modeling and Analysis of Solids and Structures. Cambridge University Press, 2009. ISBN: 978-0-511-60151-4.

[4] Alfa Laval. Gasketed plate-and-frame heat exchangers. 2016. URL: https://www.alfalaval.com/products/heat-transfer/plate-heat-exchangers/gasketed-plate-and-frame-heat-exchangers/ (visited on 04/13/2022).

[5] Alfa Laval. History of Alfa Laval. 2016. URL: https://www.alfalaval.com/about-us/our-company/history-of-alfa-laval/ (visited on 04/13/2022).

[6] Niels Ottosen and Hans Petersson. Introduction to the finite element method. Prentice Hall, 1992. ISBN: 978-0-13-473877-2.

[7] Niels Saabye Ottosen and Matti Ristinmaa. The Mechanics of Constitutive Modelling. Elsevier Science, 2005. ISBN: 978-0-08-044606-6.

[8] Matti Ristinmaa. Introduction to Non-linear Finite Element Method. Division of Solid Mechanics, Lund University, 2020.

[9] Rastko R. Šelmić and Frank L. Lewis. CHAPTER 20 - Neural Network Approximation of Piecewise Continu Ed. by Naresh K. Sinha and Madan M. Gupta. Academic Press, 2000. ISBN: 9780126464900.

Appendix A Result plots

The plots in this appendix show normalized contact pressure where 1 represents the maximum contact pressure for each plot. This has been done due to confidentiality.

A.1 Half plane width

All the plots below are associated with the half plane width parameter.

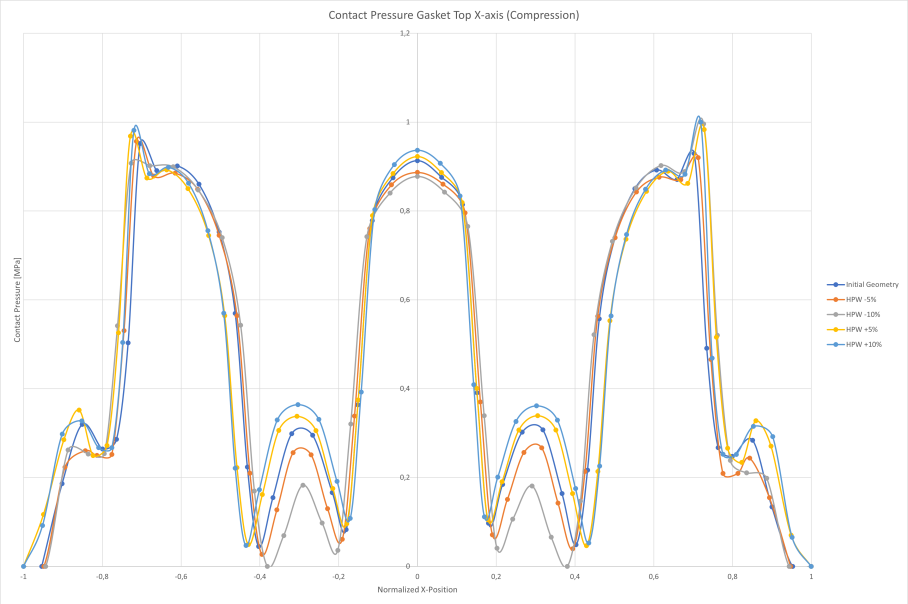

Contact Pressure for top X-axis with the NBRP rubber compound gasket, plotted after the compression step

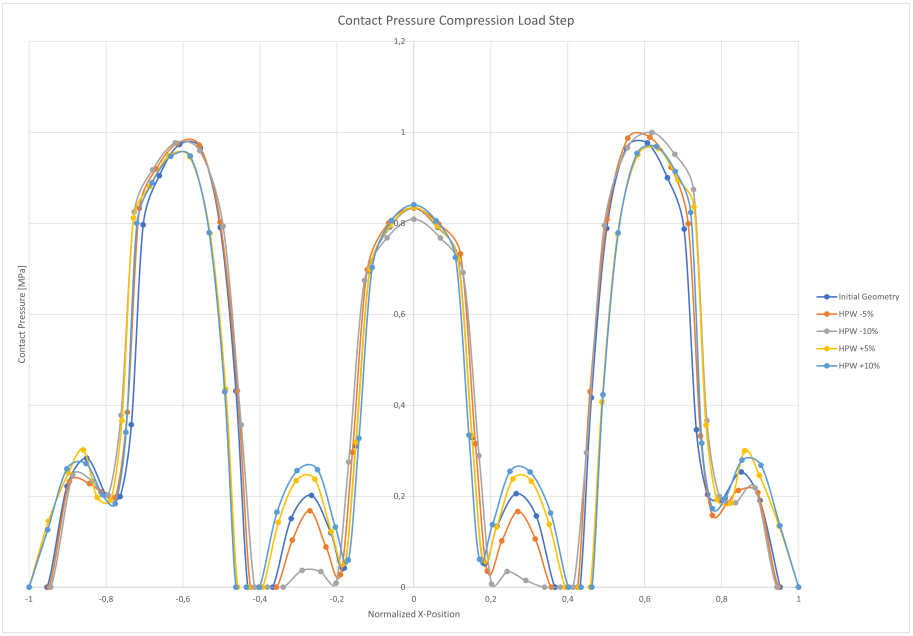

Contact Pressure for top X-axis with the EPDM rubber compound gasket, plotted after the compression step

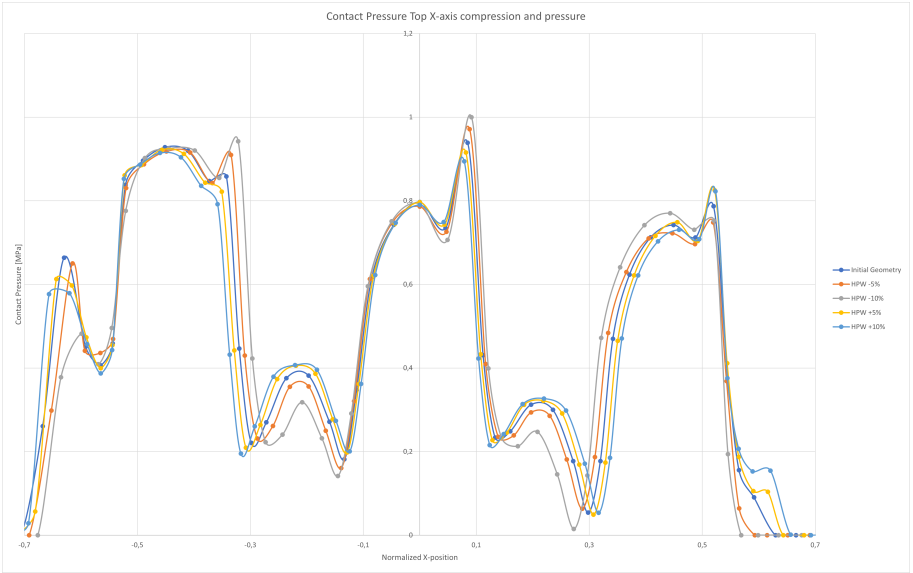

Contact Pressure for top X-axis with the NBRP rubber compound gasket, plotted after the pressurization step

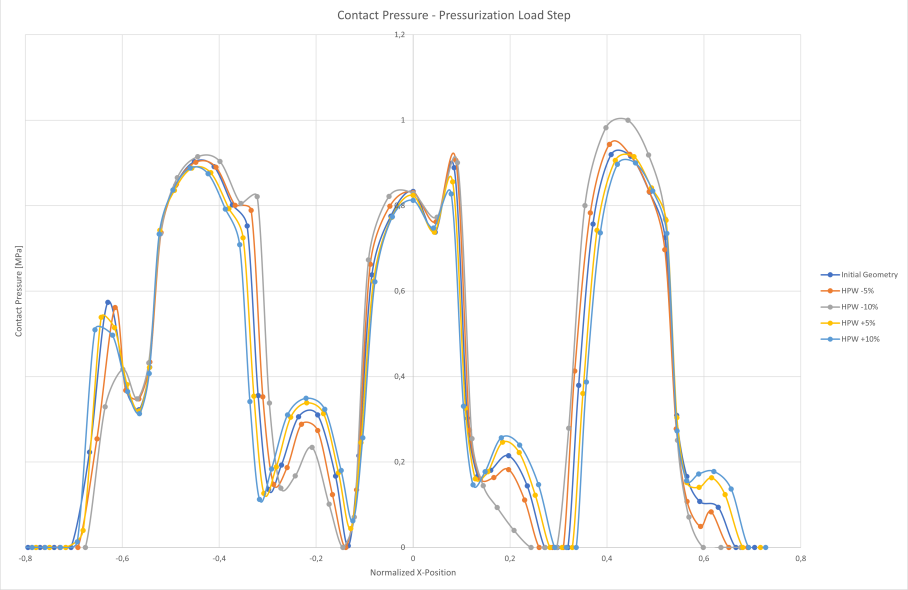

Contact Pressure for top X-axis with the EPDM rubber compound gasket, plotted after the pressurization step

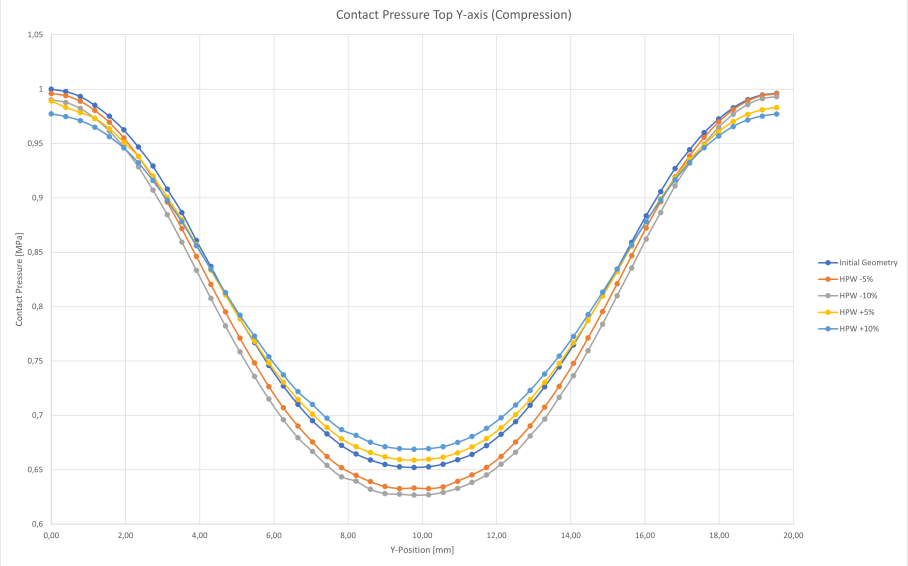

Contact Pressure for top Y-axis with the NBRP rubber compound gasket, plotted after the compression step

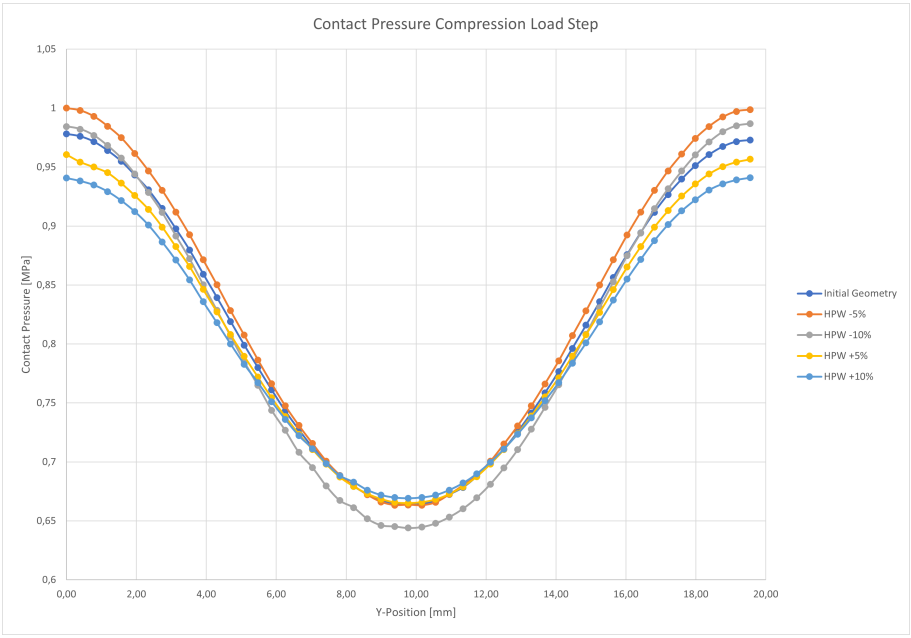

Contact Pressure for top Y-axis with the EPDM rubber compound gasket, plotted after the compression step

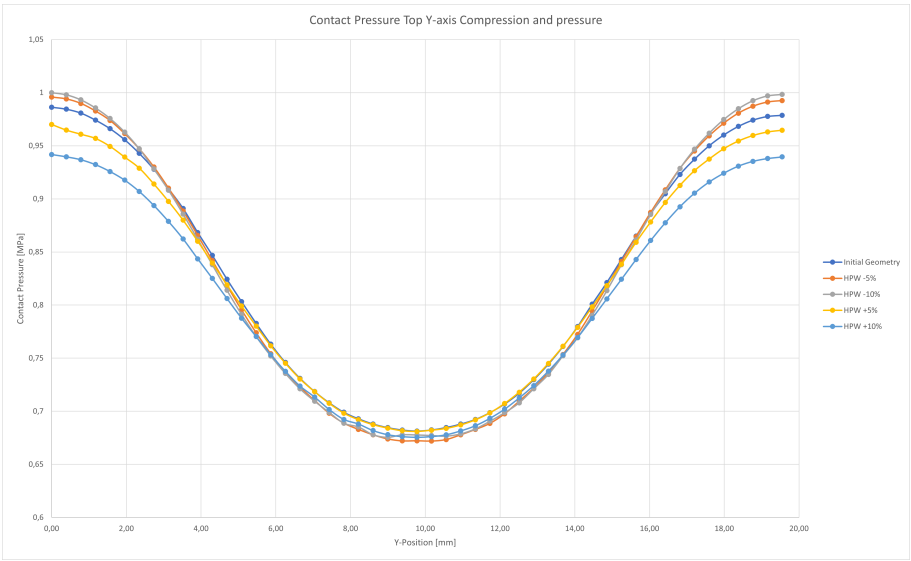

Contact Pressure for top Y-axis with the NBRP rubber compound gasket, plotted after the pressurization step

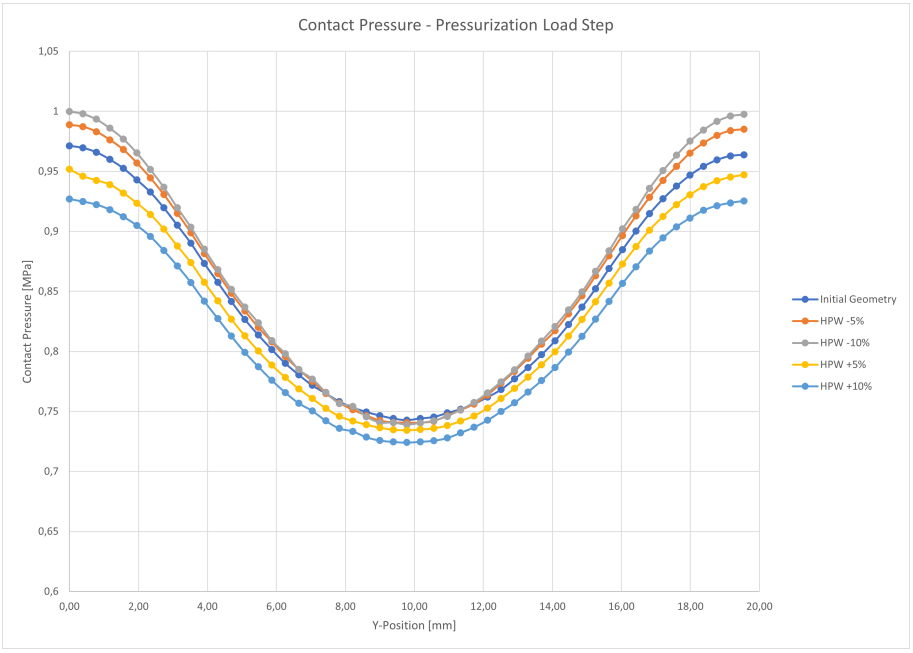

Contact Pressure for top Y-axis with the EPDM rubber compound gasket, plotted after the pressurization step

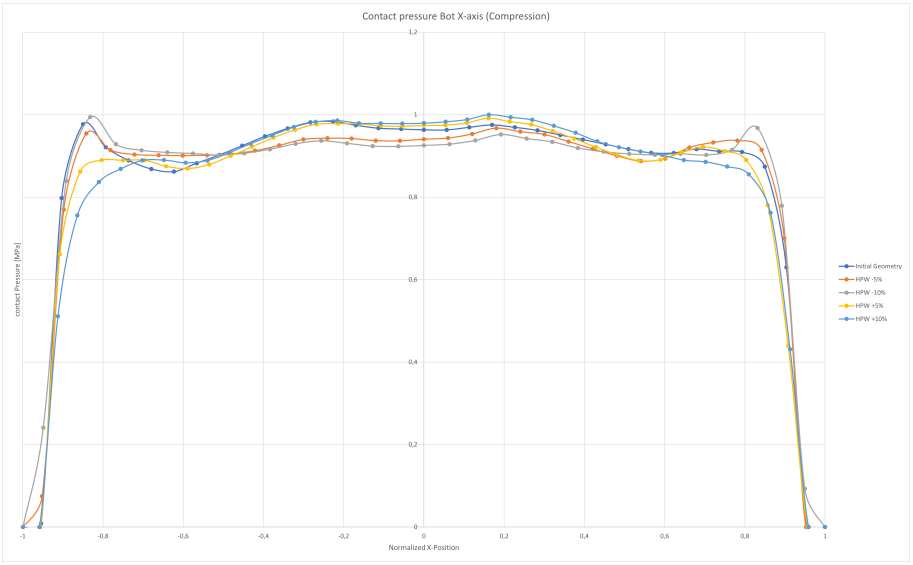

Contact Pressure for bot X-axis with the NBRP rubber compound gasket, plotted after the compression step

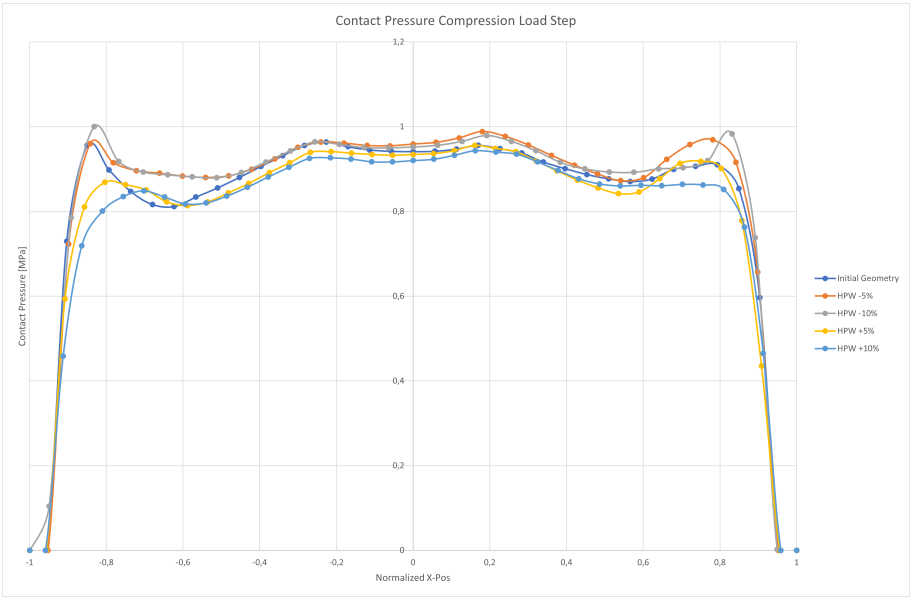

Contact Pressure for bot X-axis with the EPDM rubber compound gasket, plotted after the compression step

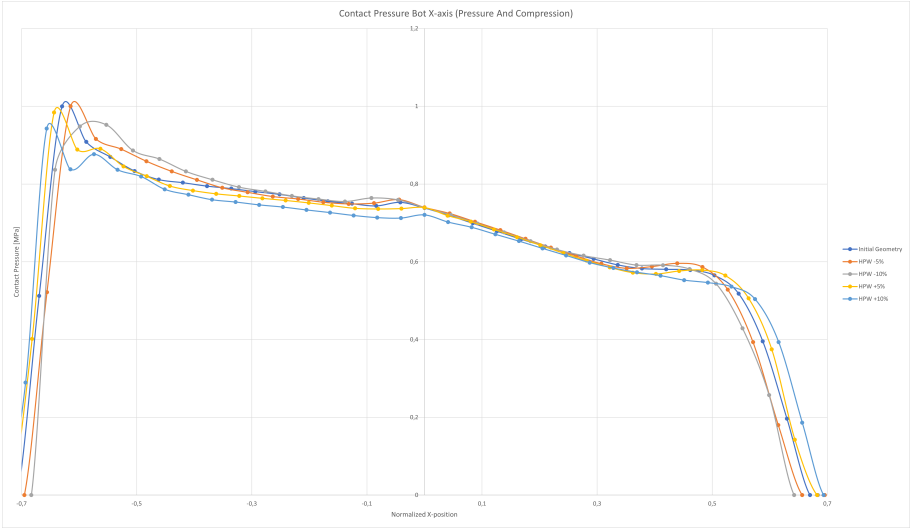

Contact Pressure for bot X-axis with the NBRP rubber compound gasket, plotted after the pressurization step

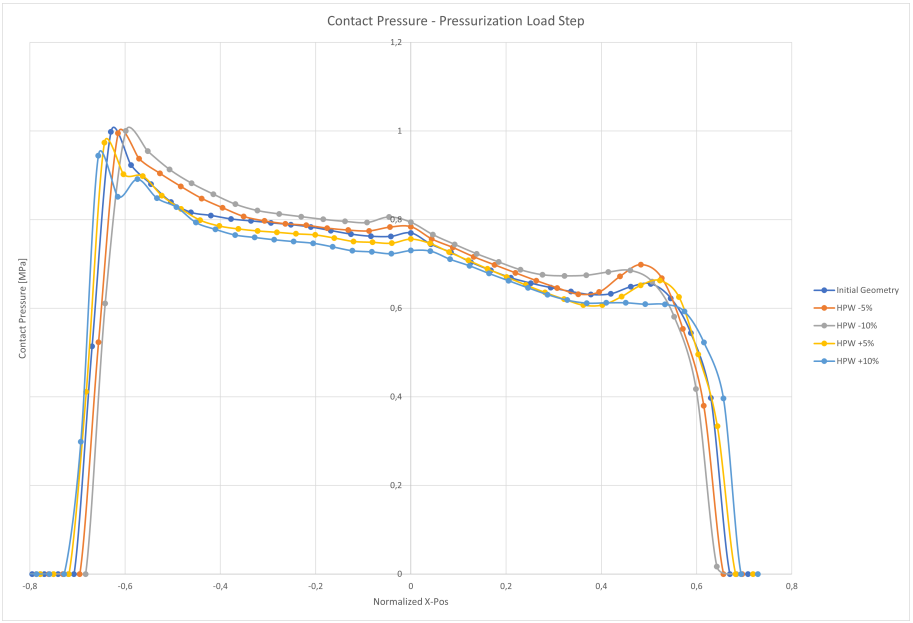

Contact Pressure for bot X-axis with the EPDM rubber compound gasket, plotted after the pressurization step

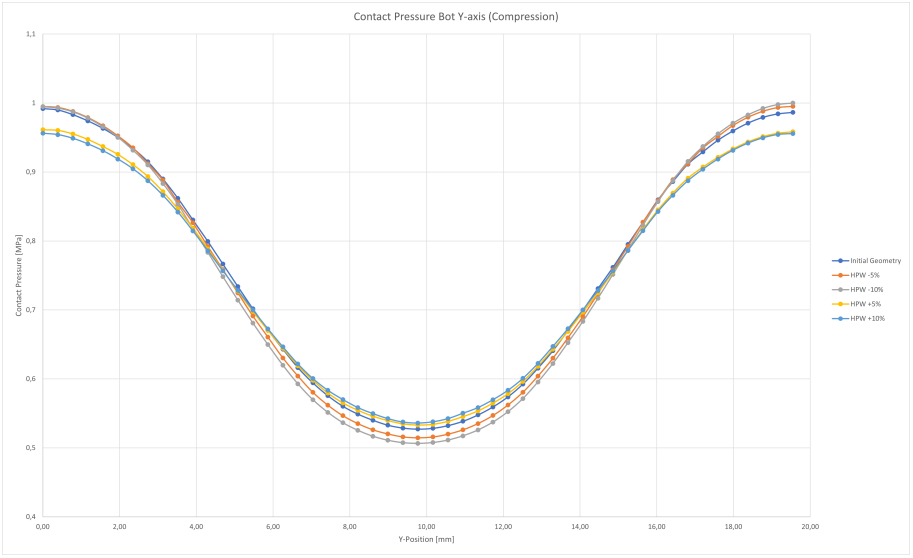

Contact Pressure for bot Y-axis with the NBRP rubber compound gasket, plotted after the compression step

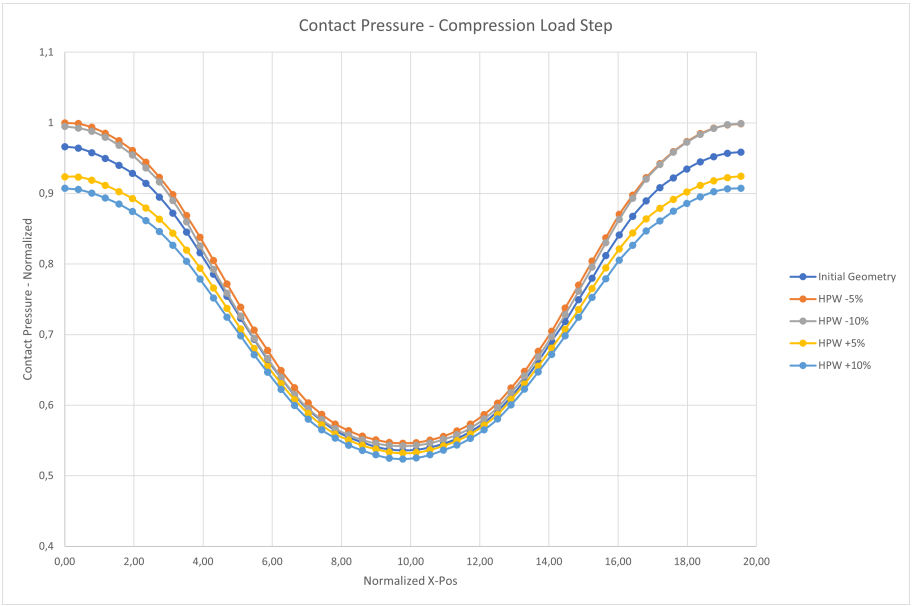

Contact Pressure for bot Y-axis with the EPDM rubber compound gasket, plotted after the compression step

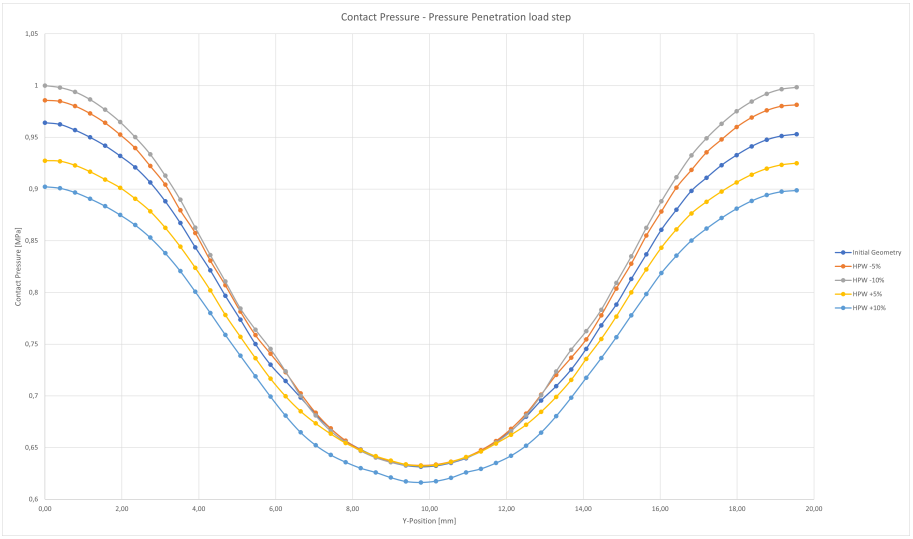

Contact Pressure for bot Y-axis with the NBRP rubber compound gasket, plotted after the pressurization step

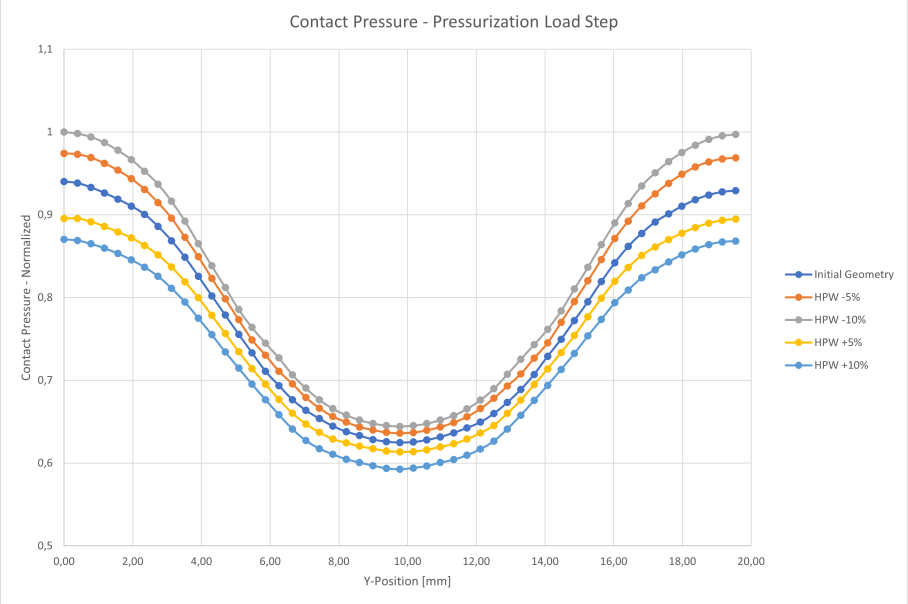

Contact Pressure for bot Y-axis with the EPDM rubber compound gasket, plotted after the pressurization step

A.2 Flank angle

All the plots below are associated with the flank angle parameter.

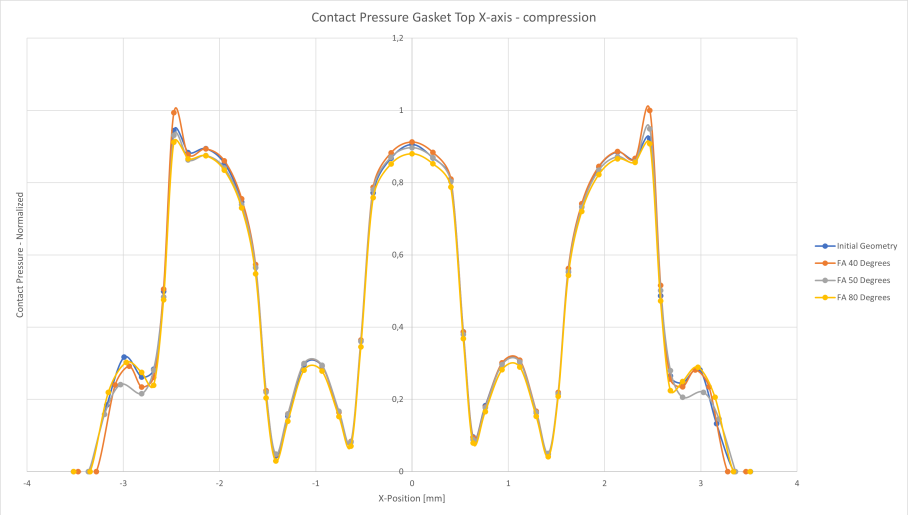

Contact pressure for top x-axis with the NBRP rubber compound gasket, plotted after the compression load step

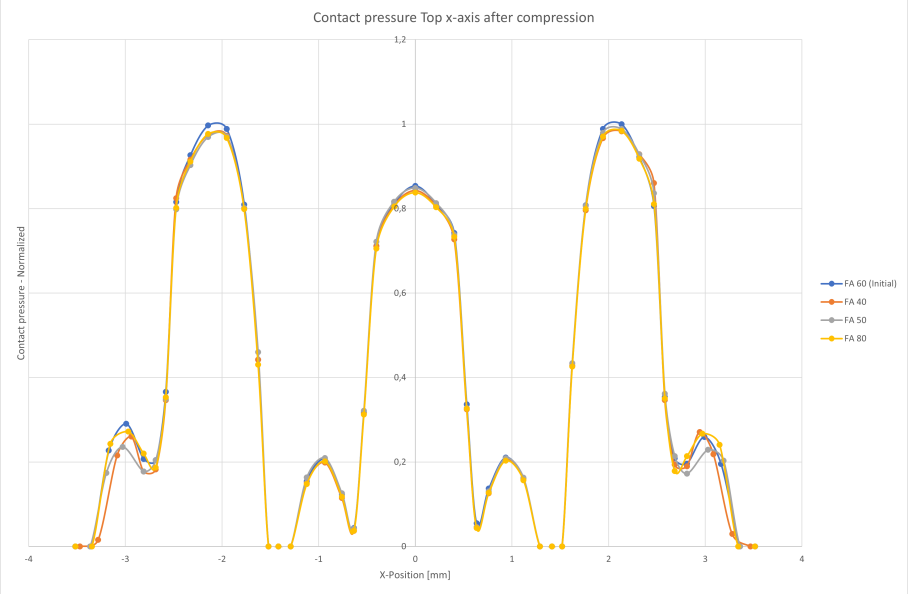

Contact pressure for top x-axis with the EPDM rubber compound gasket, plotted after the compression load step

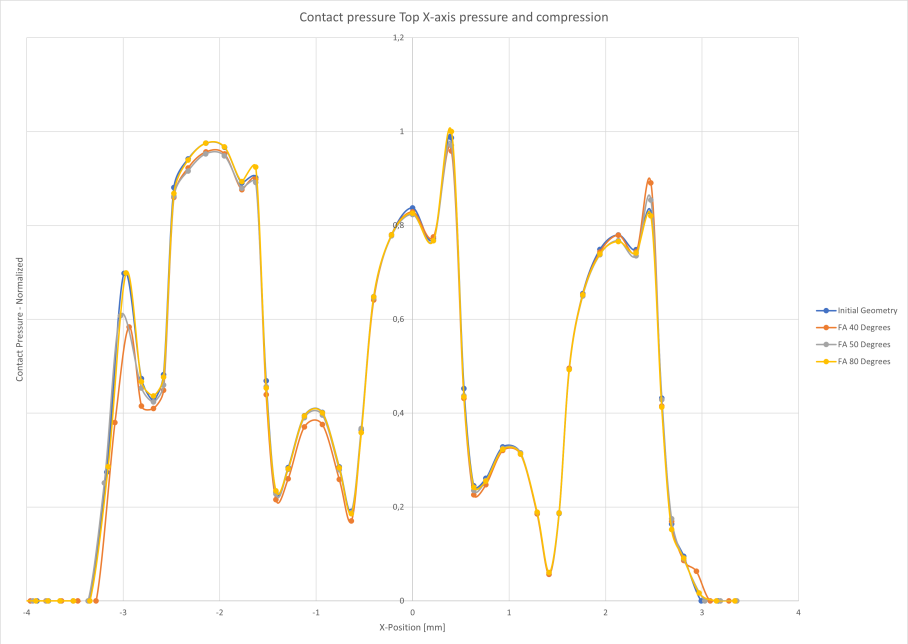

Contact pressure for top x-axis with the NBRP rubber compound gasket, plotted after the pressurization load step

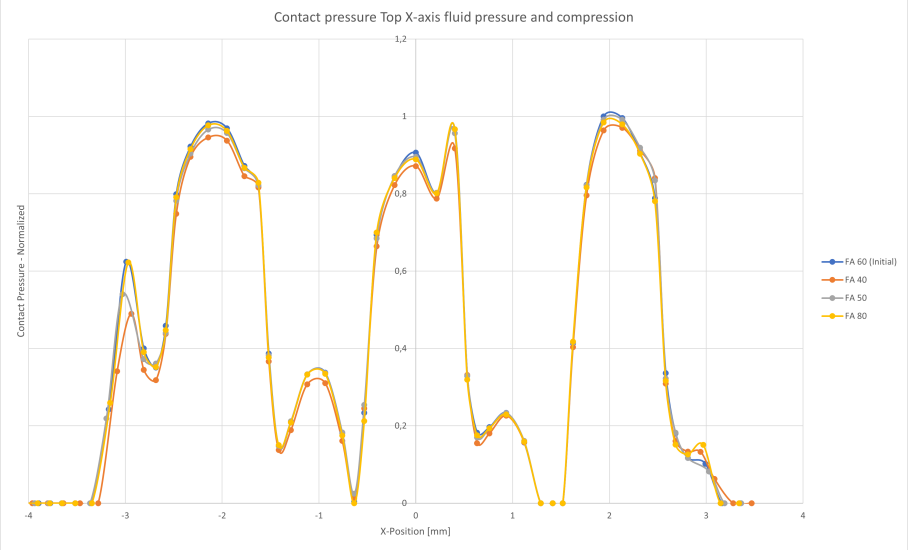

Contact pressure for top x-axis with the EPDM rubber compound gasket, plotted after the pressurization load step

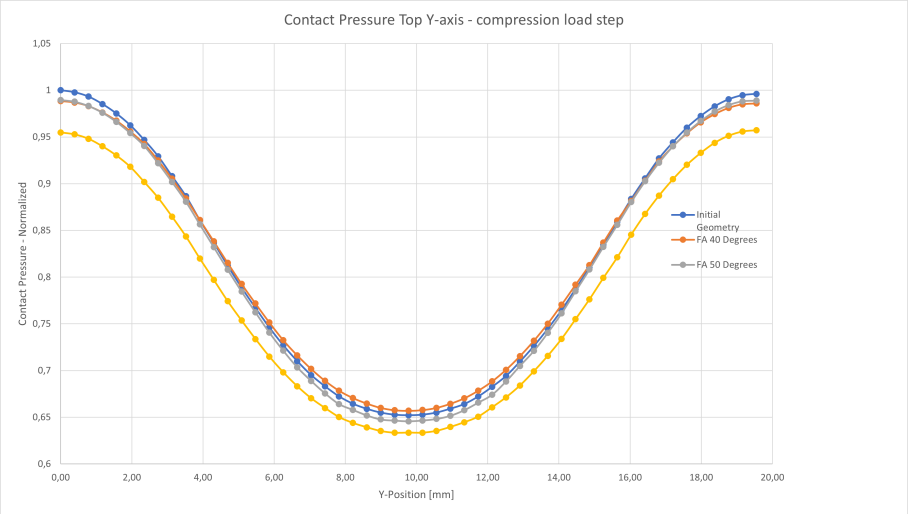

Contact pressure for top y-axis with the NBRP rubber compound gasket, plotted after the compression load step

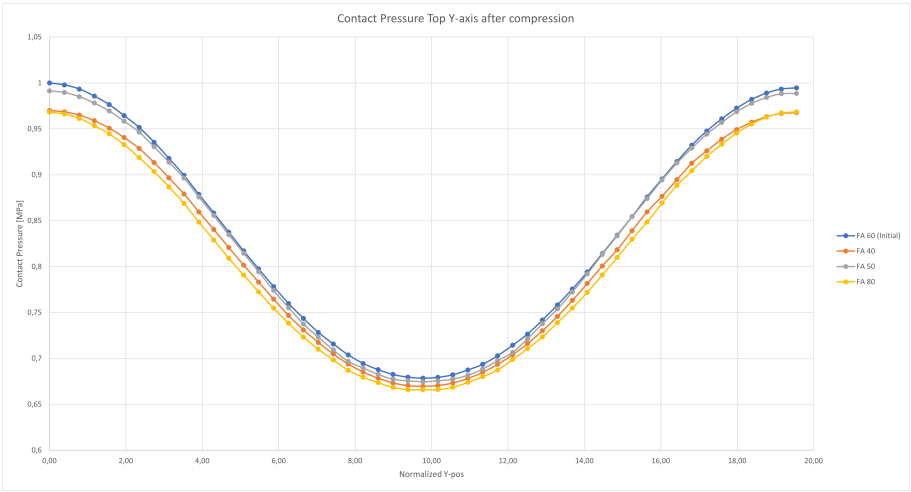

Contact pressure for top y-axis with the EPDM rubber compound gasket, plotted after the compression load step

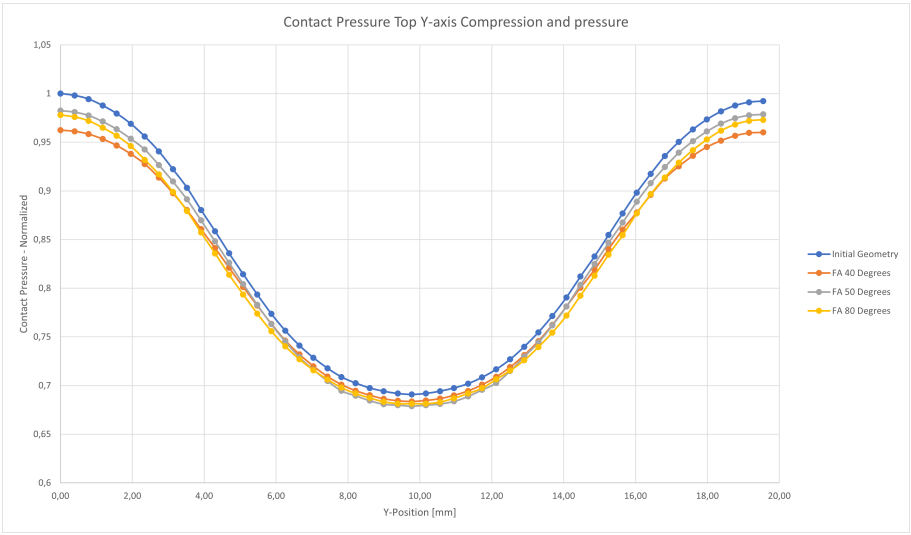

Contact pressure for top y-axis with the NBRP rubber compound gasket, plotted after the pressurization load step

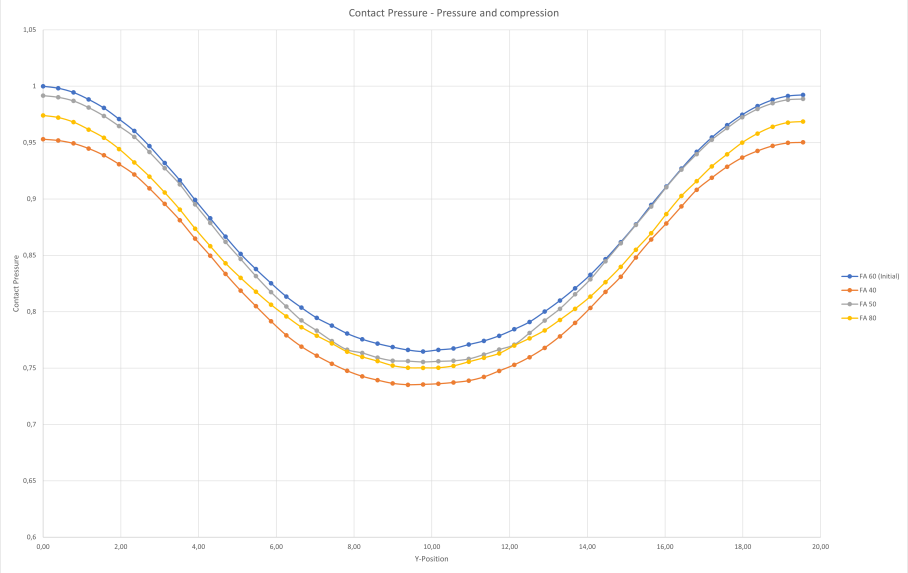

Contact pressure for top y-axis with the EPDM rubber compound gasket, plotted after the pressurization load step

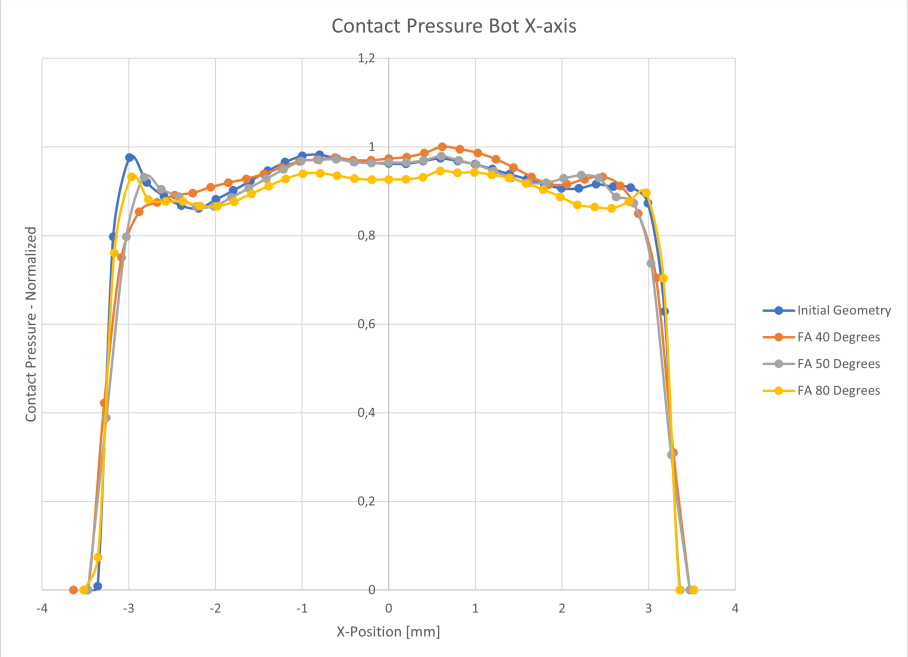

Contact pressure for bot x-axis with the NBRP rubber compound gasket, plotted after the compression load step

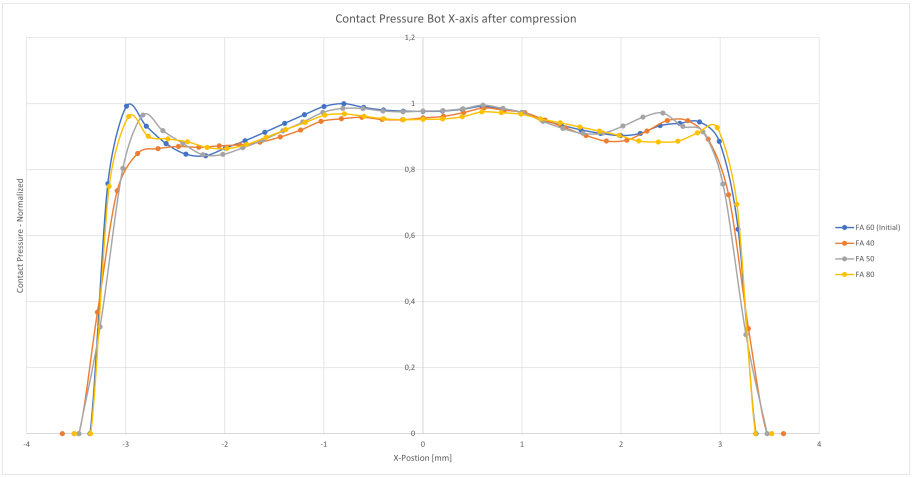

Contact pressure for bot x-axis with the EPDM rubber compound gasket, plotted after the compression load step

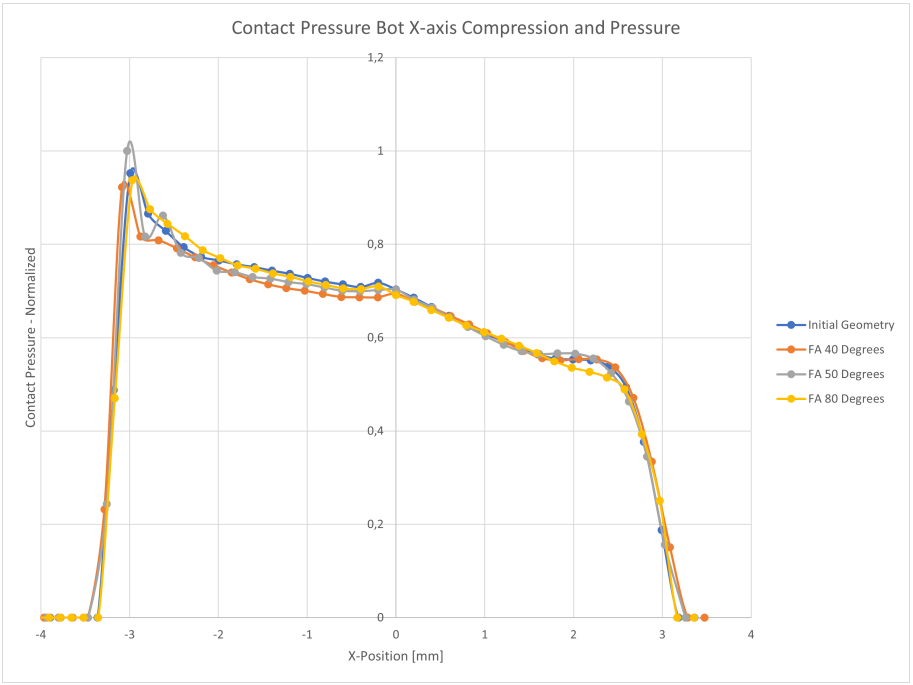

Contact pressure for bot x-axis with the NBRP rubber compound gasket, plotted after the pressurization load step

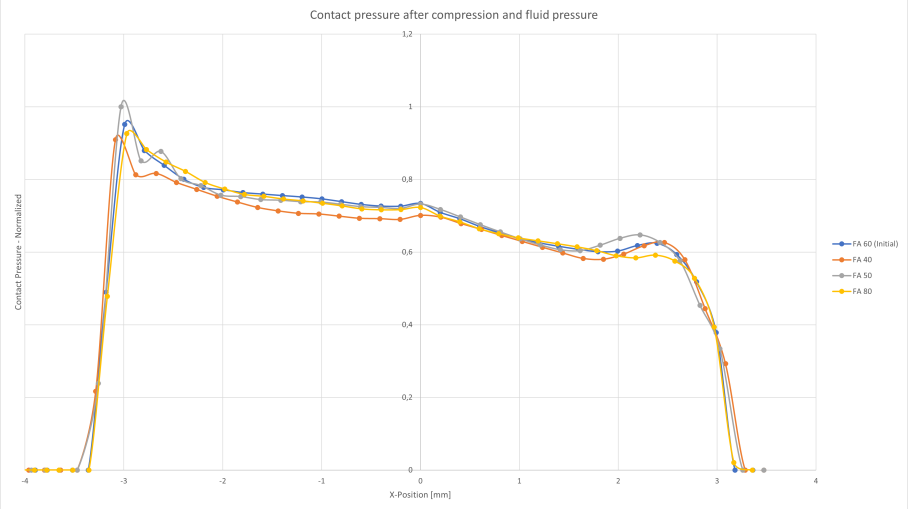

Contact pressure for bot x-axis with the EPDM rubber compound gasket, plotted after the pressurization load step

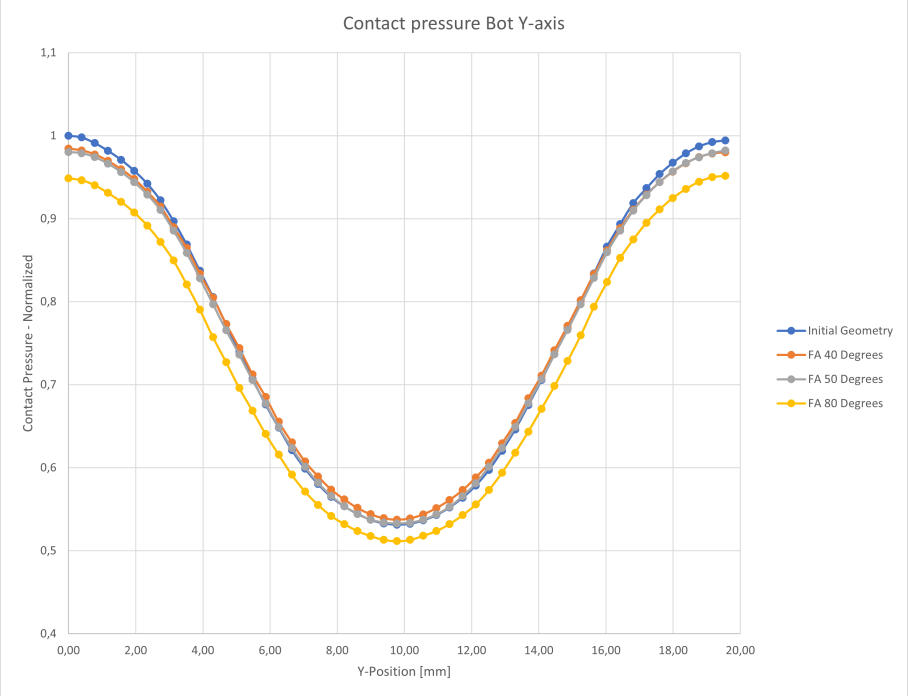

Contact pressure for bot y-axis with the NBRP rubber compound gasket, plotted after the compression load step

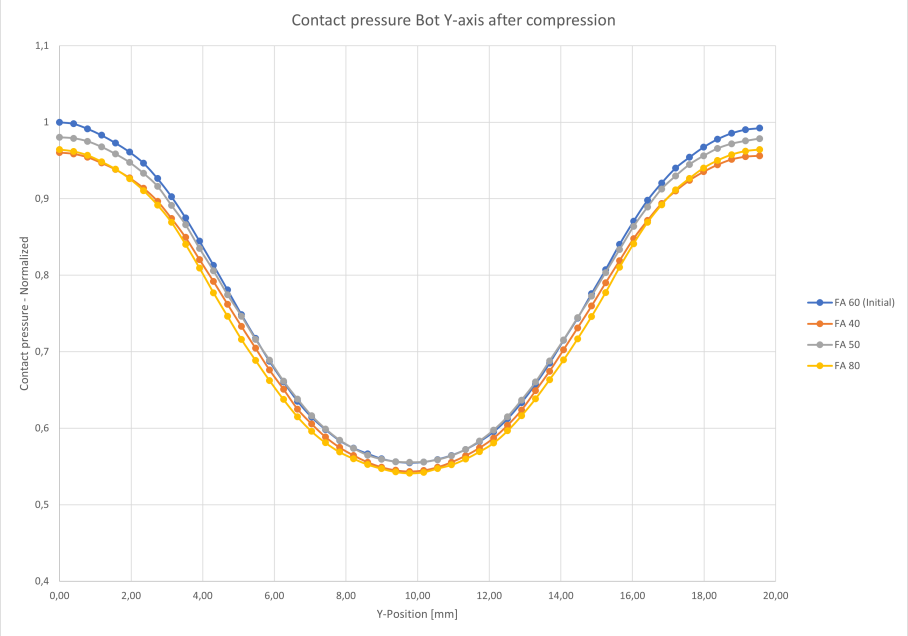

Contact pressure for bot y-axis with the EPDM rubber compound gasket, plotted after the compression load step

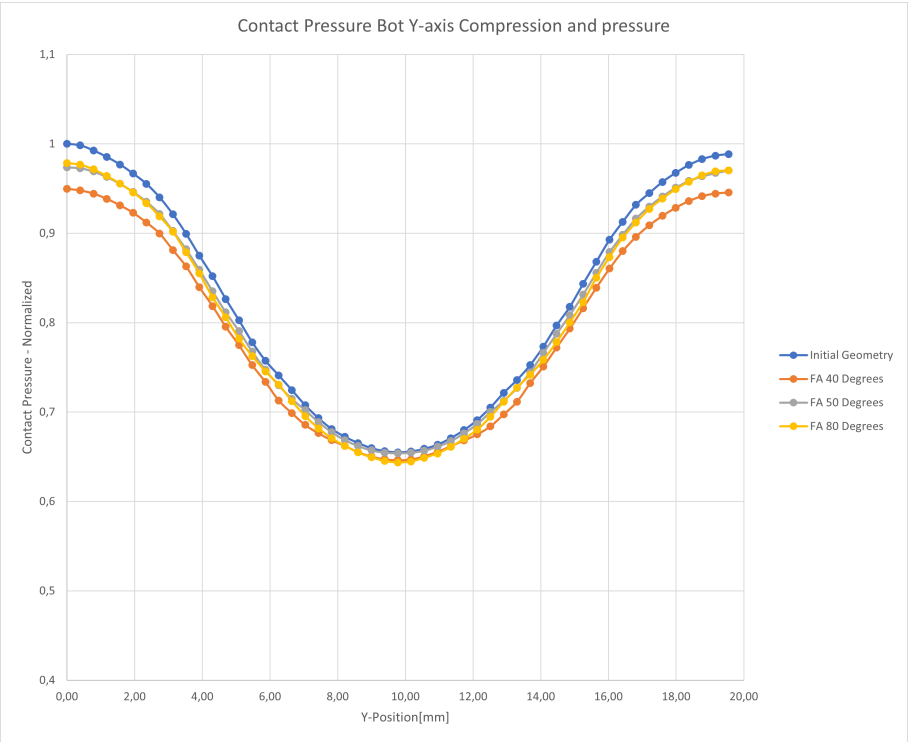

Contact pressure for bot y-axis with the NBRP rubber compound gasket, plotted after the pressurization load step

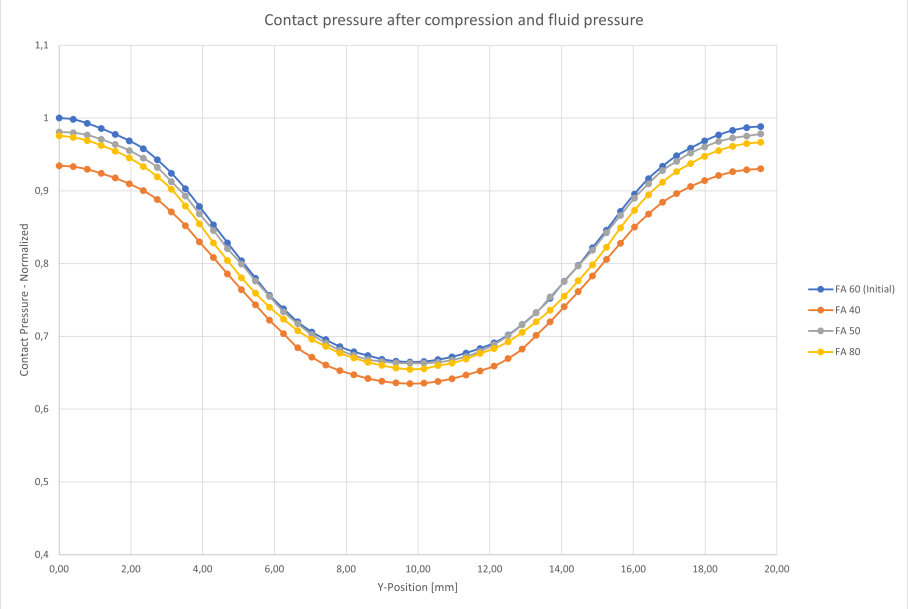

Contact pressure for bot y-axis with the EPDM rubber compound gasket, plotted after the pressurization load step

A.3 Pitch

The results presented in this section are associated with the pitch parameter.

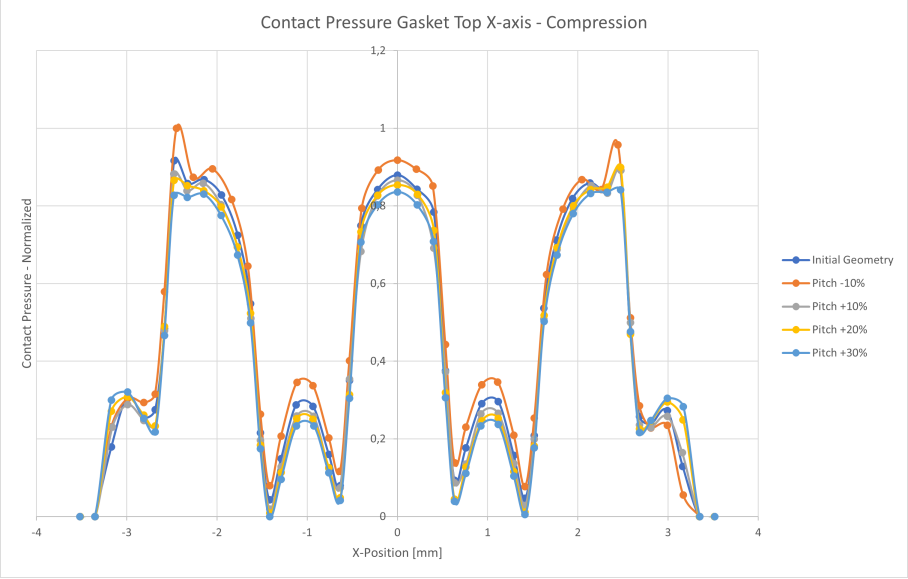

Contact Pressure for top X-axis with the NBRP rubber compound gasket, plotted after the compression step

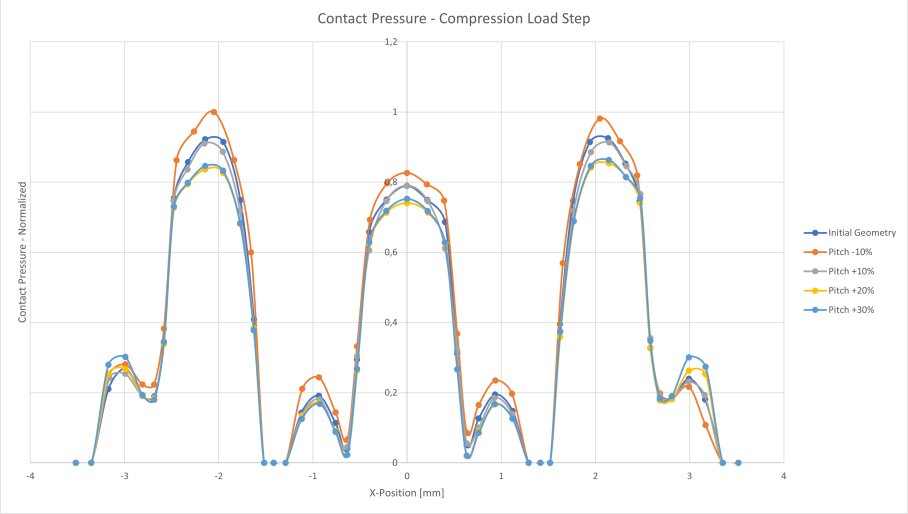

Contact Pressure for top X-axis with the EPDM rubber compound gasket, plotted after the compression step

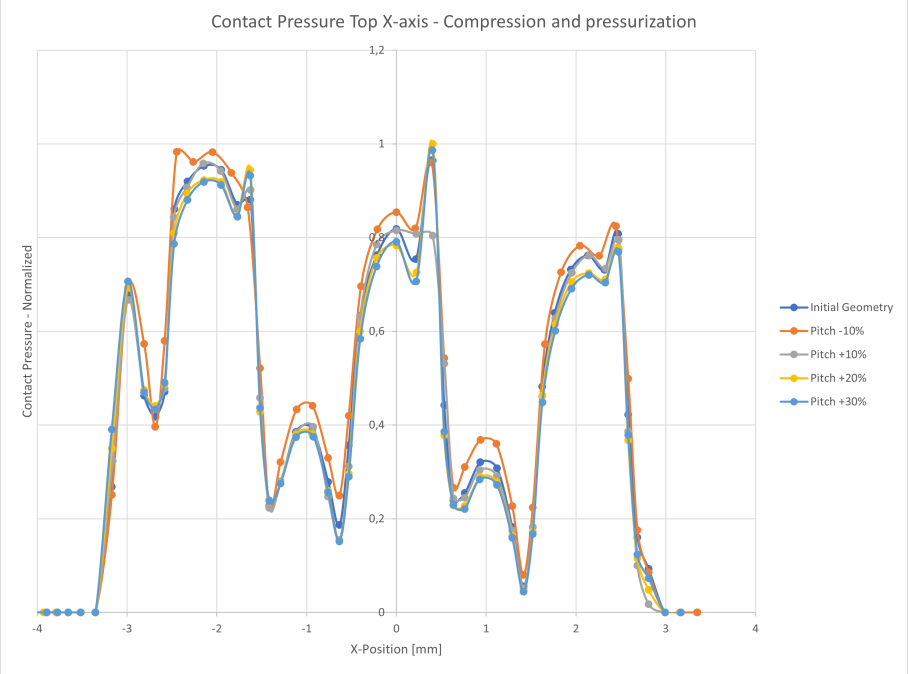

Contact Pressure for top X-axis with the NBRP rubber compound gasket, plotted after the pressurization step

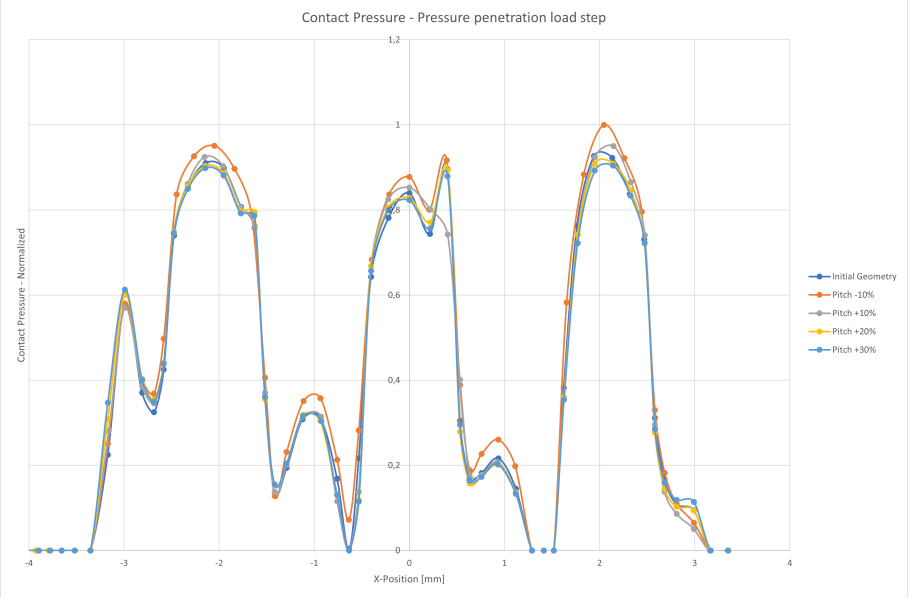

Contact Pressure for top X-axis with the EPDM rubber compound gasket, plotted after the pressurization step

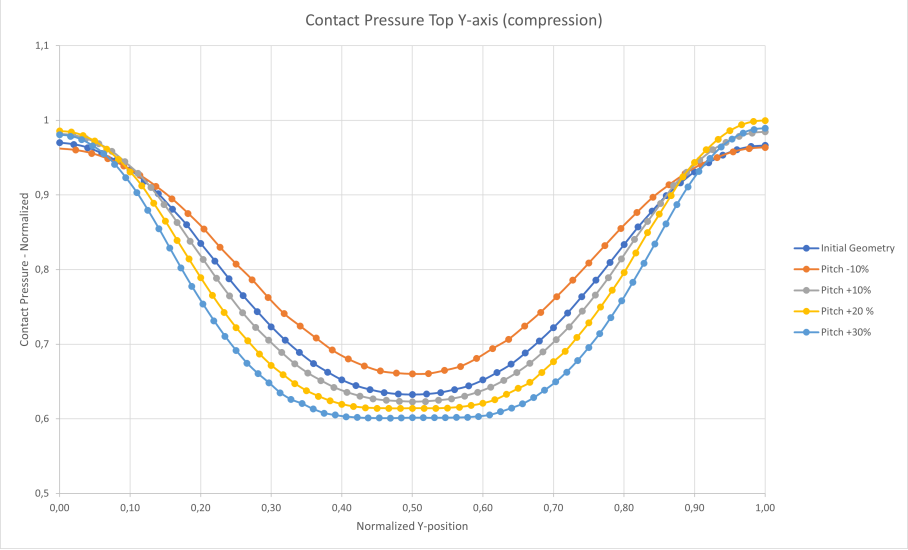

Contact Pressure for top Y-axis with the NBRP rubber compound gasket, plotted after the compression step

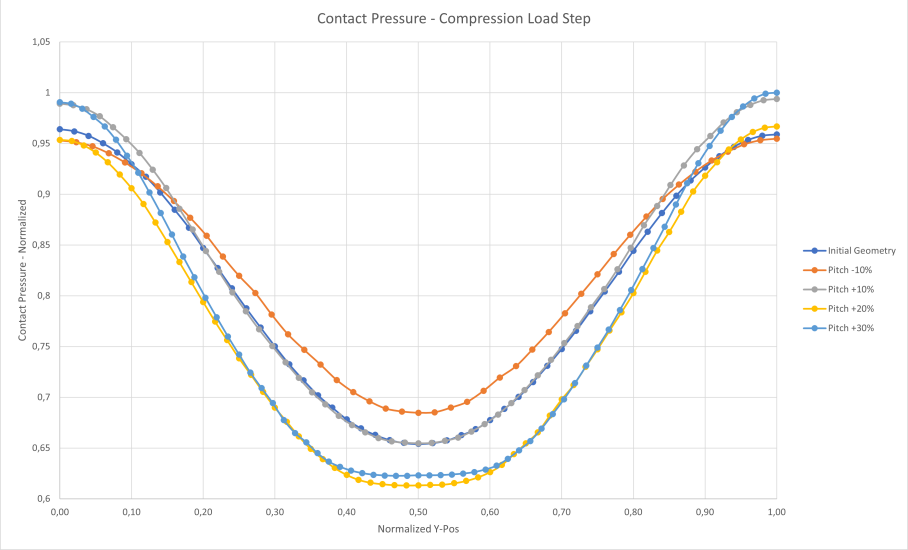

Contact Pressure for top Y-axis with the EPDM rubber compound gasket, plotted after the compression step

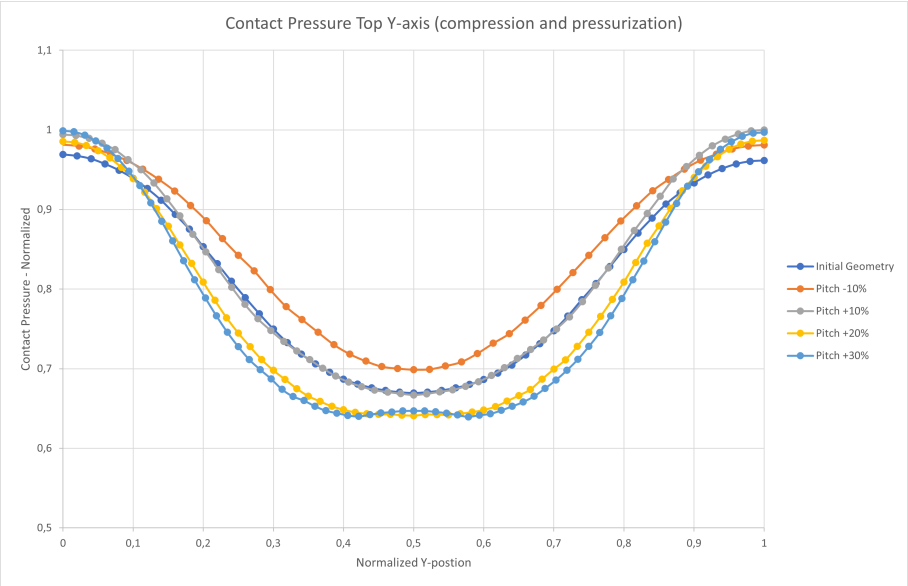

Contact Pressure for top Y-axis with the NBRP rubber compound gasket, plotted after the pressurization step

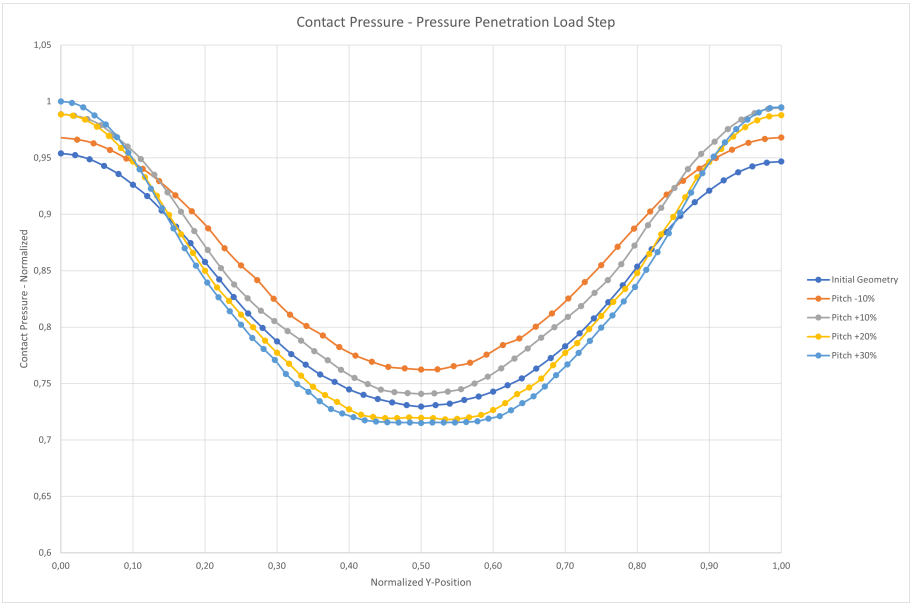

Contact Pressure for top Y-axis with the EPDM rubber compound gasket, plotted after the pressurization step

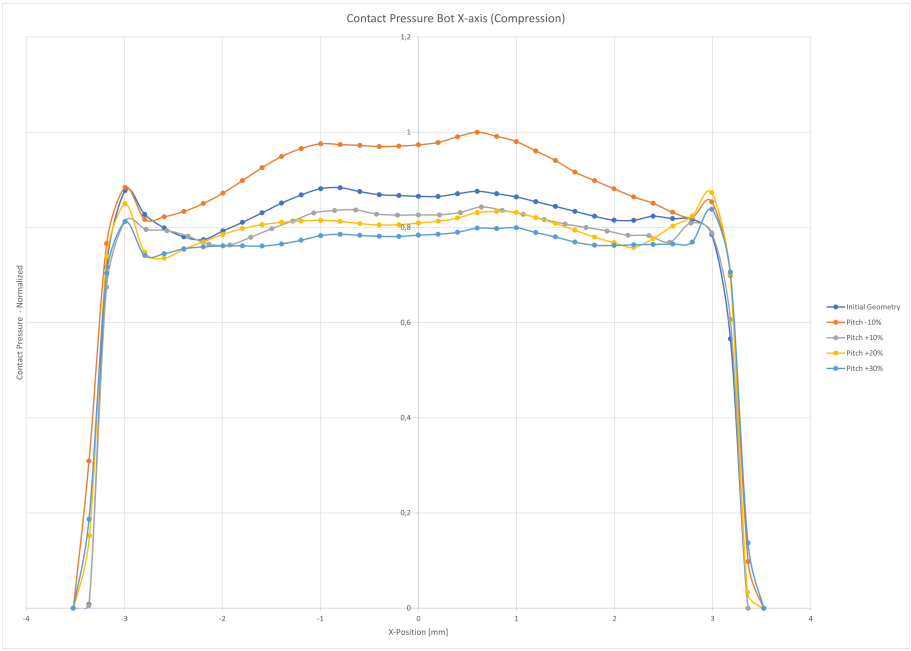

Contact Pressure for bot X-axis with the NBRP rubber compound gasket, plotted after the compression step

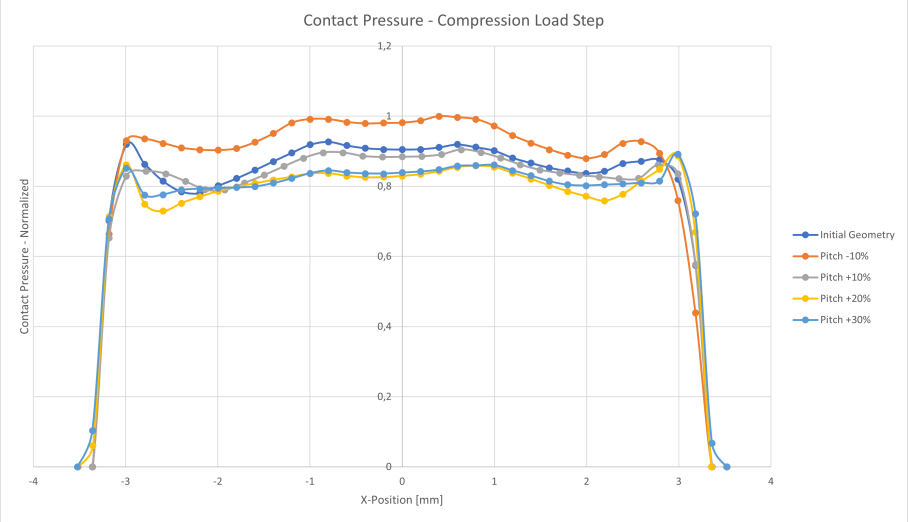

Contact Pressure for bot X-axis with the EPDM rubber compound gasket, plotted after the compression step

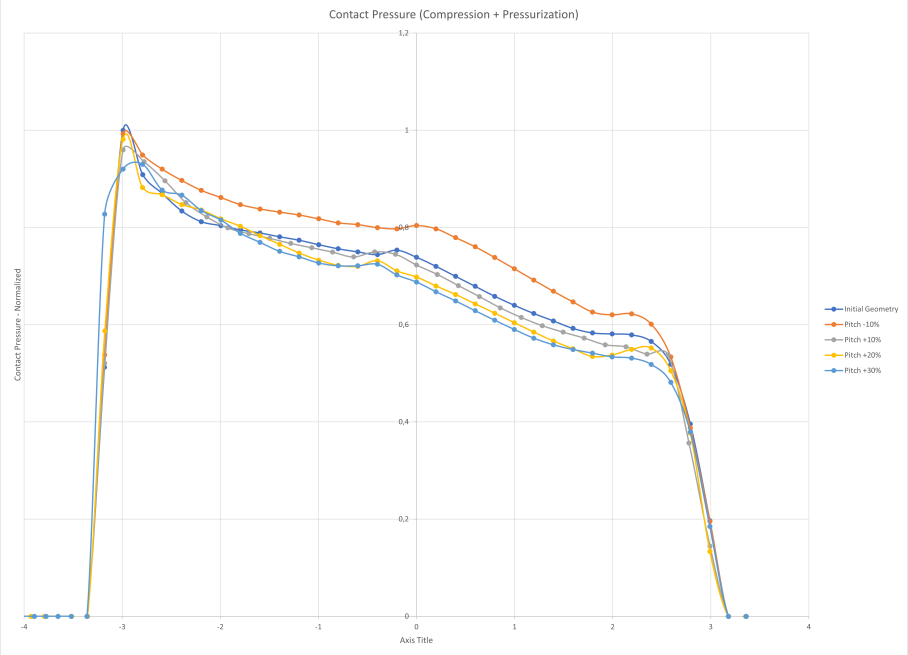

Contact Pressure for bot X-axis with the NBRP rubber compound gasket, plotted after the pressurization step

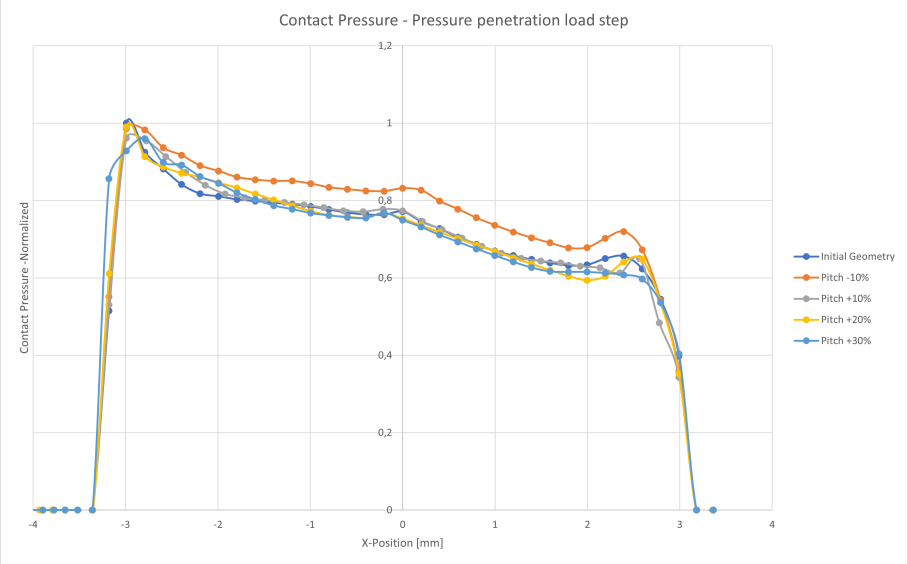

Contact Pressure for bot X-axis with the EPDM rubber compound gasket, plotted after the pressurization step

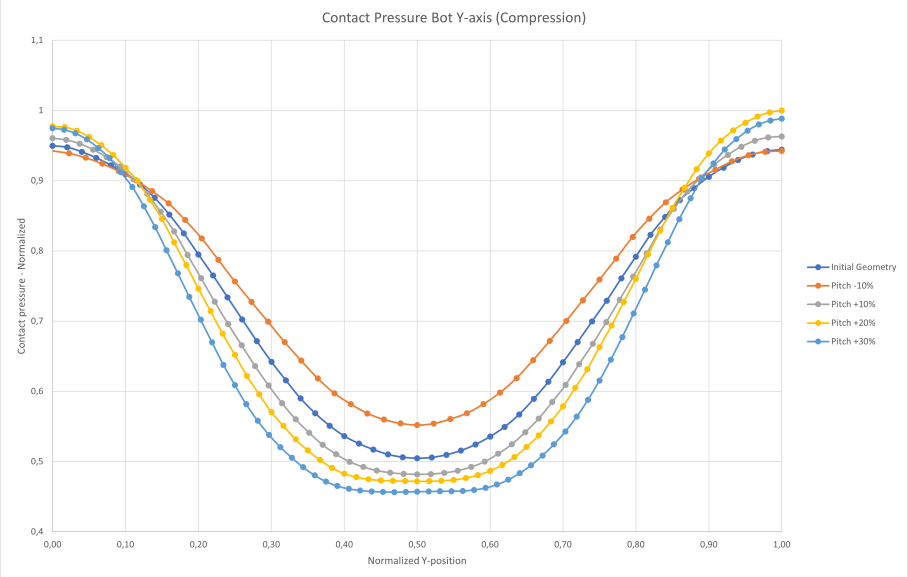

Contact Pressure for bot Y-axis with the NBRP rubber compound gasket, plotted after the compression step

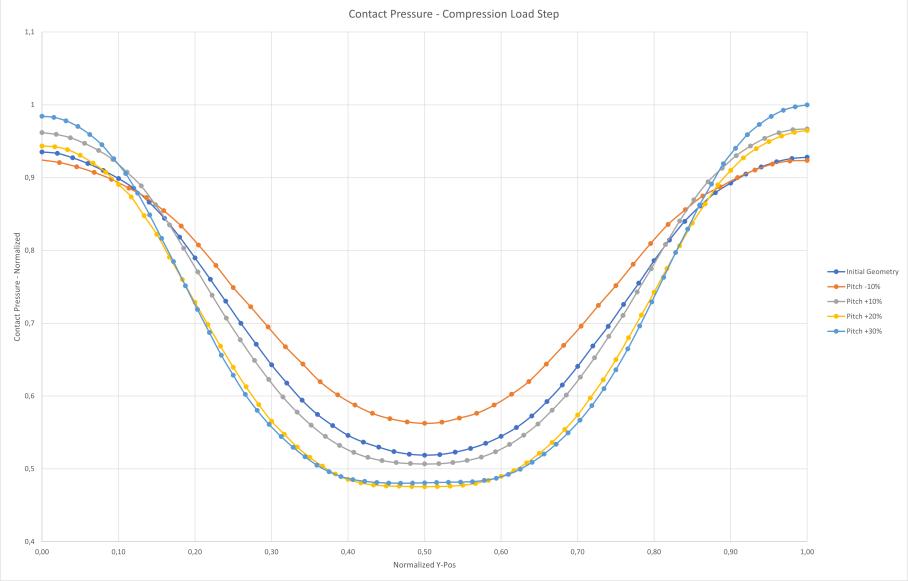

Contact Pressure for bot Y-axis with the EPDM rubber compound gasket, plotted after the compression step

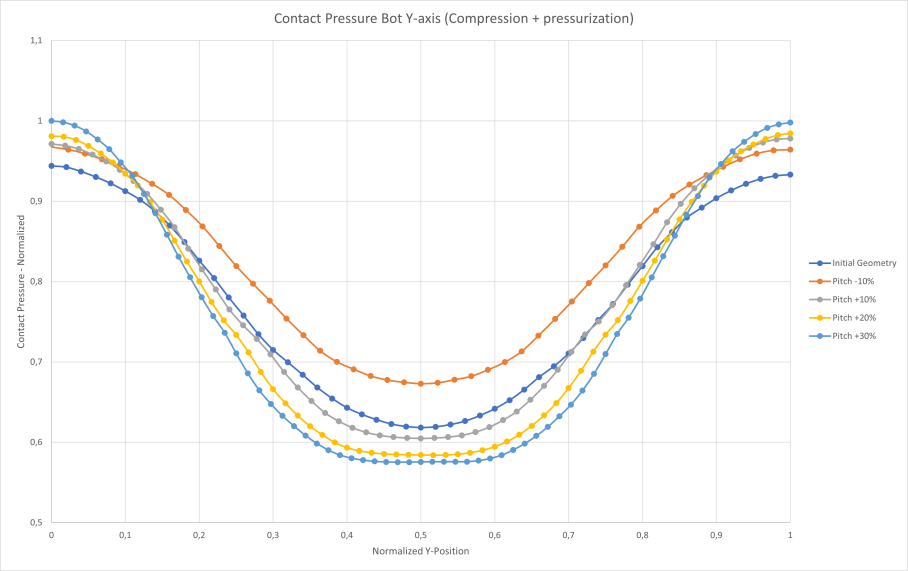

Contact Pressure for bot Y-axis with the NBRP rubber compound gasket, plotted after the pressurization step

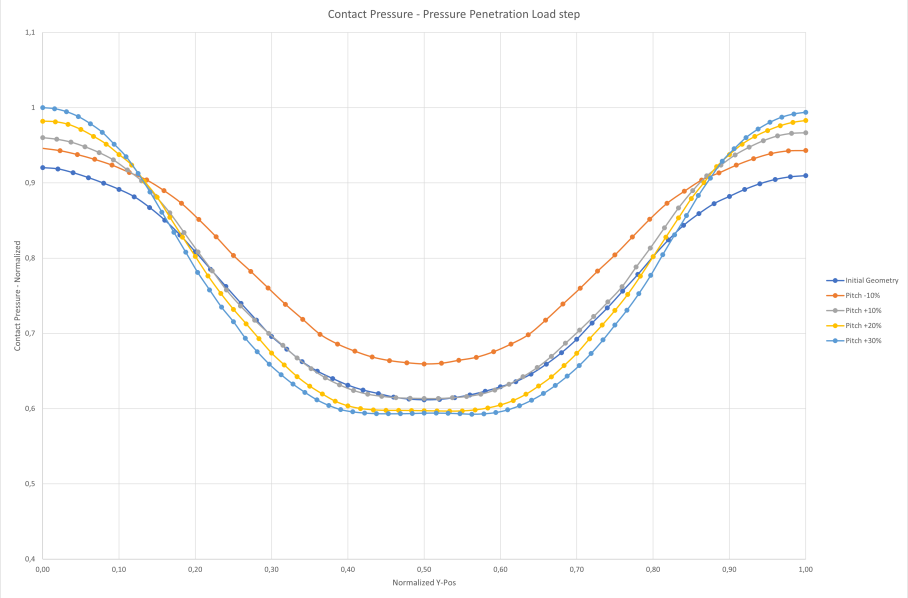

Contact Pressure for bot Y-axis with the EPDM rubber compound gasket, plotted after the pressurization step